Chapter 3

Analytical properties of the ideal MHD equations

In this chapter we discuss analytical properties of the ideal MHD equations which are useful for the interpretation and analysis of numerical simulation results throughout this dissertation. In Sec. 3.1 we introduce the ideal MHD equations. In Sec. 3.2 we discuss the theory of characteristics applied to the ideal MHD system. In the final section we introduce the theory of MHD discontinuities, and we discuss non-convexity and compound shocks.

3.1 The ideal MHD equations

The ideal MHD equations can be written under several different forms, each of which enlightens certain properties of the MHD system. First we discuss a formulation which gives insight in the physical forces and processes involved. Next the conservative form is discussed, which emphasizes the conservation law nature of the equations.

3.1.1 'Physical' form of the MHD equations

In the non-relativistic limit the dynamics of a perfectly conducting one-component fluid can be described by the ideal MHD equations. At a given point in space and time the fluid can be described by eight *state variables* (or *primitive variables*): the density ρ, pressure p, velocity vector $\vec{v}$ and magnetic field vector $\vec{B}$. These state variables are functions of the continuous space coordinate vector $\vec{x}$ and the time t. A full description of the dynamical evolution of the conducting fluid is given by eight equations which express the time evolution of the state variables.

The first equation is the mass continuity equation

$$\frac{\partial \rho}{\partial t} + \nabla \cdot (\rho \vec{v}) = 0, \tag{3.1}$$

which describes the conservation of mass. This equation is the same as for the case of a neutral fluid.

Three more equations are provided by the vector momentum equation

$$\rho \frac{d\vec{v}}{dt} = -\nabla p + (\nabla \times \vec{B}) \times \vec{B}, \tag{3.2}$$

which is an expression of Newton's law of motion. This equation is the same as for the case of a neutral fluid, except for the additional $\vec{J} \times \vec{B}$ force exerted by the magnetic field on the charged fluid elements. The current density $\vec{J}$ is given by Ampère's law

$$\vec{J} = \nabla \times \vec{B}, \tag{3.3}$$

with units chosen such that the magnetic permeability μ equals 1 and does thus not show up in the equations. The relation between the total or convective derivative d/dt (which can be thought of as to describe the time evolution of a quantity associated with a moving fluid element) and the partial or local derivative $\partial/\partial t$ is given by

$$\frac{d}{dt} = \frac{\partial}{\partial t} + (\vec{v} \cdot \nabla). \tag{3.4}$$

The next three equations are given by the vector induction equation

$$\frac{\partial \vec{B}}{\partial t} = \nabla \times (\vec{v} \times \vec{B}), \tag{3.5}$$

which derives directly from one of Maxwell's equations, namely, Faraday's law of induction, and from Ohm's law for an ideal plasma

$$\vec{E} = -\vec{v} \times \vec{B}, \tag{3.6}$$

with $\vec{E}$ the electric field.

The final equation describes the evolution of the pressure

$$\frac{\partial p}{\partial t} + (\vec{v} \cdot \nabla) p + \gamma p \nabla \cdot \vec{v} = 0, \tag{3.7}$$

where ideal gas behavior is assumed. This equation is the same as for the case of a neutral fluid, and describes the conservation of the specific entropy s. Indeed, we can rewrite Eq. 3.7 as

$$\frac{ds}{dt} = 0, \tag{3.8}$$

with the (specific) entropy s given by

$$s = \frac{p}{\rho^\gamma}, \tag{3.9}$$

for an ideal gas. We call s the entropy throughout this dissertation, although strictly speaking the thermodynamic entropy density is given by the quantity $c_v \log(s)$, with c_v the specific heat at constant volume. The adiabatic index γ is the ratio of specific heats, and is taken equal to the mono-atomic gas value of $5/3$ throughout this dissertation, because the ion component of most space physics plasmas mainly consists of ionized hydrogen.

This constitutes a complete system of evolution equations describing the dynamics of a conducting fluid. However, it is an observational fact that magnetic monopoles do not exist in nature, so the above equations have to be supplemented with the divergence free condition

$$\nabla \cdot \vec{B} = 0. \tag{3.10}$$

This condition implies that the magnetic flux is conserved in space, in the sense that the net flux through the surface of a closed volume vanishes, which allows for the concept of *flux tubes*. By taking the divergence of the induction equation 3.5 one can see that once the divergence free condition is imposed as an initial condition, it automatically remains fulfilled at later times. The divergence free condition is thus in a way *compatible* with the MHD equations, and can be seen as an additional *constraint* to the MHD system.

3.1.2 Conservative form of the MHD equations

The MHD equations introduced above can be re-stated in explicit conservation law form. We introduce the specific total energy e, given by

$$e = \frac{p}{\gamma - 1} + \rho \frac{\vec{v} \cdot \vec{v}}{2} + \frac{\vec{B} \cdot \vec{B}}{2}. \tag{3.11}$$

Then the ideal MHD equations can be written as

$$\frac{\partial}{\partial t} \begin{bmatrix} \rho \\ \rho \vec{v} \\ \vec{B} \\ e \end{bmatrix} + \nabla \cdot \begin{bmatrix} \rho \vec{v} \\ \rho \vec{v}\vec{v} + \mathsf{I}\left(p + \vec{B} \cdot \vec{B}/2\right) - \vec{B}\vec{B} \\ \vec{v}\vec{B} - \vec{B}\vec{v} \\ \left(e + p + \vec{B} \cdot \vec{B}/2\right)\vec{v} - \left(\vec{v} \cdot \vec{B}\right)\vec{B} \end{bmatrix} = - \begin{bmatrix} 0 \\ \vec{B} \\ \vec{v} \\ \vec{v} \cdot \vec{B} \end{bmatrix} \nabla \cdot \vec{B}. \tag{3.12}$$

This form of the equations expresses the basic conservation of the *conservative variables* mass ρ, momentum $\rho\vec{v}$, magnetic field $\vec{B}$ and specific total energy e, and shows explicitly that the total mass, momentum, magnetic field and energy present in any given volume can only change when there is a net *flux* through the boundaries of the volume. This equation again has to be supplemented with the divergence free condition $\nabla \cdot \vec{B} = 0$ as an initial condition.

The right hand side (RHS) term of Eq. 3.12 is proportional to $\nabla \cdot \vec{B} = 0$ and is thus identically zero, but for several reasons to be explained below it is advantageous to keep this term in the equations.

The main function of the RHS term (sometimes also called the *Powell source term*) is that it makes the MHD equations *Galilean invariant* also when $\nabla \cdot \vec{B} \neq 0$. A necessary property of any well-posed theory in non-relativistic physics is that it has to be Galilean invariant. The MHD system, for instance as described by the equations given in Sec. 3.1.1 supplemented with the $\nabla \cdot \vec{B} = 0$ condition, of course is Galilean invariant. However, without this constraint, the induction equation 3.5 of Sec. 3.1.1 is *not* Galilean invariant, as can be shown as follows [34]. Making the following Galilean transformation to a new rest frame indicated by primed quantities

$$\begin{aligned} \vec{x}\,' &= \vec{x} - \vec{a}t \\ t' &= t \\ \vec{v}\,' &= \vec{v} - \vec{a} \\ \vec{B}\,' &= \vec{B} \\ \frac{\partial}{\partial t} &= \frac{\partial}{\partial t'} - \vec{a} \cdot \nabla' \\ \nabla &= \nabla', \end{aligned} \tag{3.13}$$

the induction equation Eq. 3.5 transforms to

$$\frac{\partial \vec{B}\,'}{\partial t'} = \nabla' \times (\vec{v}\,' \times \vec{B}\,') - \vec{a}\,\nabla' \cdot \vec{B}\,', \tag{3.14}$$

which is clearly of a different form than Eq. 3.5 (if $\nabla \cdot \vec{B} \neq 0$). We can restore Galilean invariance by changing the induction equation 3.5 to

$$\frac{\partial \vec{B}}{\partial t} = \nabla \times (\vec{v} \times \vec{B}) - \vec{v}\,\nabla \cdot \vec{B}, \tag{3.15}$$

and this is precisely the form of the induction equation in Eq. 3.12. If one does not use the $\nabla \cdot \vec{B} = 0$ condition in rewriting the equation of motion Eq. 3.2 into conservative form, then one finds the form of Eq. 3.12 with the extra RHS source term. Similarly, construction of the total energy equation without making use of the $\nabla \cdot \vec{B} = 0$ condition leads to the

form with the RHS source term. We can thus summarize by saying that the conservative form of the equations *without* the RHS source term is *not* Galilean invariant when $\nabla \cdot \vec{B} \neq 0$, but that the form *with* the source term restores Galilean invariance.

Although $\nabla \cdot \vec{B} = 0$ rigorously in analytical approaches to MHD problems, it is useful to consider the form of the equations with the source term in the following three cases.

First, Godunov [51, 52, 7] proved in 1972 that this is the unique form of the MHD equations which is symmetrizable. The symmetrized form of the equations is useful for the design of numerical schemes in natural 'entropy variables' [7] and for the analysis of stability of shock waves [35].

Second, we show in Sec. 3.2 that the inclusion of this RHS term is essential for our derivation of the characteristic theory of the MHD equations in a simple, compact, and systematic procedure using a matrix approach. Characteristic analysis based on the symmetrizable form of the conservative MHD equations gives insight into the basic structure of the MHD equations as a system of Galilean invariant conservation laws with a constraint.

Third, in some numerical schemes, the $\nabla \cdot \vec{B} = 0$ constraint is only satisfied up to a discretization error. As first shown in [118], inclusion of the RHS term assures that these small $\nabla \cdot \vec{B}$ errors are consistently accounted for in a numerically stable way and do not lead to accumulation of inaccuracies. The numerical code used in this dissertation makes use of this technique to control the $\nabla \cdot \vec{B}$ errors, as is described in Chapter 4.

Next to the conservation of mass, momentum, magnetic field and energy mentioned above, there are other quantities in the ideal MHD system which are conserved in the sense that they are *frozen* into the moving plasma. As follows from Eq. 3.9, the entropy s of a moving fluid element is a conserved scalar quantity. Also, the *magnetic flux* through a surface moving with the flow is a conserved quantity associated with the magnetic field lines which are frozen into the plasma. Indeed, we can make use of a general expression for the convective time derivative of the flux Φ of a vector field $\vec{A}$ through a surface S which moves with velocity $\vec{u}$. The flux Φ is defined by

$$\Phi = \int_S \vec{A} \cdot \vec{n} dS, \tag{3.16}$$

with $\vec{n}$ the vector normal to the surface, and the total time derivative of the flux is given by

$$\frac{d\Phi}{dt} = \int_S (\frac{\partial \vec{A}}{\partial t} + \vec{u}(\nabla \cdot \vec{A}) + \nabla \times (\vec{A} \times \vec{u})) \cdot \vec{n} dS. \tag{3.17}$$

The total time derivative of the flux Φ_B of the magnetic field $\vec{B}$ through a surface moving with the plasma speed $\vec{v}$ is then given by

$$\frac{d\Phi_B}{dt} = \int_S (\frac{\partial \vec{B}}{\partial t} + \vec{v}(\nabla \cdot \vec{B}) + \nabla \times (\vec{B} \times \vec{v})) \cdot \vec{n} dS. \tag{3.18}$$

Using the Galilean invariant form of the induction equation Eq. 3.15 it follows that the magnetic flux Φ_B through a surface moving with the plasma is conserved *in time*

$$\frac{d\Phi_B}{dt} = 0, \tag{3.19}$$

also if $\nabla \cdot \vec{B} \neq 0$. It is interesting to remark that the conserved variables ρ, $\rho\,\vec{v}$, $\vec{B}$ and e remain conserved quantities in dissipative MHD (Eq. 2.6), whereas the entropy s and the magnetic flux are not conserved (frozen–in) in dissipative MHD. Another manifestation of the fact that the magnetic field is frozen into the plasma for ideal MHD, is that fluid elements which reside on a common field line at one time, remain on this magnetic field line at all times. These frozen-in quantities can be characterized and classified with more insight when one considers them in the framework of differential forms, vector fields and Lie-derivatives, as is done for instance in [65]. The magnetic field vector, for instance, is a 2-form or an *axial* vector, which in general has the property of conservation of flux. These considerations, however, are beyond the scope of this introduction to the MHD equations.

The ideal MHD system belongs to the class of symmetric hyperbolic systems [21], which have many interesting and well-defined properties. Hyperbolic systems describe wave phenomena. Characteristic analysis naturally reveals the properties of the hyperbolicity of the system and its associated waves, and is taken up in Sec. 3.2.

3.1.3 Scaling invariance of the stationary ideal MHD equations

Physical variables are expressed in certain units, and we have some freedom in choosing these units. The solution to a given physical stationary MHD problem should of course not depend on the units we choose. We can scale the primitive variables and space coordinates as

$$\begin{aligned} \rho'(\vec{x}\,') &= \bar{\rho}\,\rho(\vec{x}) \\ p'(\vec{x}\,') &= \bar{p}\,p(\vec{x}) \\ \vec{v}\,'(\vec{x}\,') &= \bar{v}\,\vec{v}(\vec{x}) \\ \vec{B}\,'(\vec{x}\,') &= \bar{B}\,\vec{B}(\vec{x}) \\ \vec{x}\,' &= \bar{x}\,\vec{x} \end{aligned} \tag{3.20}$$

with for instance ρ' the density in the new units, ρ the original density, and $\bar{\rho}$ a scaling factor. Scaling the variables in the momentum equation 3.2 with $\partial/\partial t \equiv 0$ results in

$$\frac{\bar{p}}{\bar{\rho}\bar{v}^2}\rho'\left(\vec{v}'\cdot\nabla'\right)\vec{v}' = -\nabla' p' + \frac{\bar{p}}{\bar{B}^2}\left(\nabla'\times\vec{B}'\right)\times\vec{B}'. \tag{3.21}$$

This equation describes the same physical problem as the momentum equation 3.2 in the original variables only if $\bar{p} = \bar{\rho}\bar{v}^2$ and $\bar{p} = \bar{B}^2$. This expresses the fact that we cannot completely freely choose units because the dimensions of physical quantities are not independent. For stationary ideal MHD, these are the only two independent dimensional constraints. We call scaling under these constraints *consistent scaling*.

This reasoning also implies that every class of solutions to the stationary ideal MHD system which are equivalent up to scaling, is labeled by two independent dimensionless quantities taken in an arbitrary point of the solution, for which we can choose the following:

$$\beta = \frac{p}{B^2/2} \quad \text{and} \quad M = \frac{v}{\sqrt{\gamma p/\rho}}, \tag{3.22}$$

with v and B vector magnitudes. The reader can verify that these two quantities are indeed invariant under consistent scaling. Sometimes the Alfvénic Mach number $M_A = v/(B/\sqrt{\rho})$ is taken in stead of the sonic Mach number M. These quantities do not depend on the spatial scale, so stationary ideal MHD flows are length scale invariant. For instance, in stationary bow shock flows the size of the obstacle is irrelevant, because scaling the obstacle just means that the solution has to be scaled in the same way.

Consider a stationary ideal MHD flow problem with the boundary geometry and boundary conditions specified. We can obtain physically different flow problems by scaling the values imposed at inflow boundaries without taking into account the dimensional constraints. This non-consistent scaling changes the values of β and/or M. There are only two parameters that can be changed independently, so we can say that ideal MHD problems have *two free parameters* under scaling. If one studies stationary ideal MHD problems in a general way and one wants to perform complete parameter studies, it is important to know how many free scaling parameters there are and it is helpful to label solutions with these free parameters. Therefore most of the time we express inflow conditions in terms of the dimensionless quantities β and M for the numerical simulations described in this dissertation.

3.2 Characteristic analysis of the ideal MHD equations

An extensive general theory exists for the characteristic properties of symmetric hyperbolic systems [21, 20]. This theory has been applied early on to unsteady MHD flows [21] and to steady planar ($B_z \equiv v_z \equiv 0$) MHD flows, including the case where the magnetic field is aligned with the flow (field-aligned or parallel flow) [79, 59]. More complete accounts of the characteristic theory of steady and unsteady MHD flows appeared later [71, 85, 70, 3].

In this Section we present a concise derivation of some aspects of the characteristic theory of the MHD equations with two independent variables (time-dependent MHD in the xt plane and steady MHD in the xy plane), in preparation for the characteristic analysis of MHD flows with shocks later in this dissertation. This Section serves to introduce the reader who is unfamiliar with the theory of characteristics to the concepts, nomenclature and notation that is used further on. Moreover, our derivation of this characteristic theory, based on the Galilean invariant symmetrizable form of the conservative MHD equations with a source term [51, 118, 7] and using a matrix approach [70, 19], is new and attractive in its own right, because it gives insight into the structure of the MHD equations as a system of Galilean invariant conservation laws with a constraint, and because in a simple, compact, and systematic way we recover all the various results that are scattered throughout the literature [21, 79, 59, 71, 85, 70, 3, 19]. This derivation of characteristic theory has appeared in [151]. Before deriving the characteristic properties of the MHD system with two independent variables, we briefly introduce the concept of characteristic curves, starting from the simple case of a scalar equation.

3.2.1 The theory of characteristics

The basic concepts and definitions of characteristic theory can be most clearly presented for the simple scalar case. Consider a conservation law for the *scalar* quantity $u(x,t)$ which depends on two independent variables x and t,

$$\frac{\partial u}{\partial t} + \frac{\partial f(u)}{\partial x} = 0, \tag{3.23}$$

or

$$\frac{\partial u}{\partial t} + f'(u)\frac{\partial u}{\partial x} = 0, \tag{3.24}$$

where $f(u)$ is called the flux function and the prime denotes a derivative with respect to u. If $f'(u)$ is real, then there exist curves $x(t)$ in the xt

plane defined by

$$\frac{dx(t)}{dt} = f'(u), \tag{3.25}$$

such that

$$\frac{du(x(t),t)}{dt} = 0. \tag{3.26}$$

Along these curves, which are called characteristics, the partial differential equation Eq. 3.23 reduces to the ordinary differential equation Eq. 3.26. The equation is said to be hyperbolic when $f'(u)$ is real and real characteristic curves exist. The scalar u is then invariant on the characteristic curve and is called a Riemann Invariant (RI). The slope of the characteristic $\lambda = f'(u)$ is called the characteristic speed. For the scalar case, the characteristics are straight lines (when f only depends on u and not directly on the independent variables).

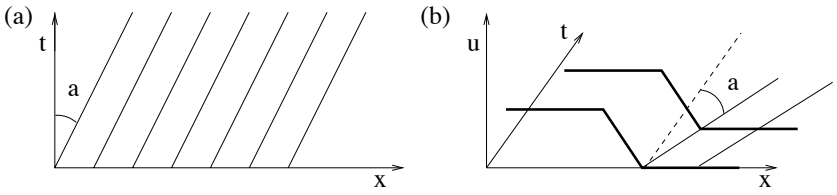

Figure 3.1: *The scalar advection equation. (a) Characteristic curves (thin solid) are parallel straight lines with slope a. (b) A wave profile u (thick solid) is advected with speed a.*

The most simple illustration of these concepts is probably the case of the *linear* scalar conservation law, with flux function $f(u) = a\,u$. The characteristics are parallel straight lines in the xt plane with slope $f'(u) = a$, as shown in Fig. 3.1a. The scalar u is constant on every characteristic, which means that a wave profile is just advected with speed a, as shown in Fig. 3.1b. A scalar conservation law with a linear flux function is therefore also called a *scalar advection equation.*

An example of a *nonlinear* scalar conservation law is Burgers' equation, with flux function $f(u) = u^2/2$. The effect of the nonlinearity of the flux function is that a smooth profile can steepen into a shock. In Fig. 3.2 we show how an initial state containing a linear profile for $x \in [0,1]$, varying from $u = 1.5$ on the left to $u = -0.5$ on the right, steepens into a shock. Fig. 3.2a shows the characteristics with slope $f'(u) = u$ in the xt plane. The shock is formed when the characteristics first intersect at $(x = 3/4, t = 1/2)$. The discontinuity is necessary to avoid a multivalued solution where the characteristics intersect. Fig. 3.2b shows a surface plot of u.

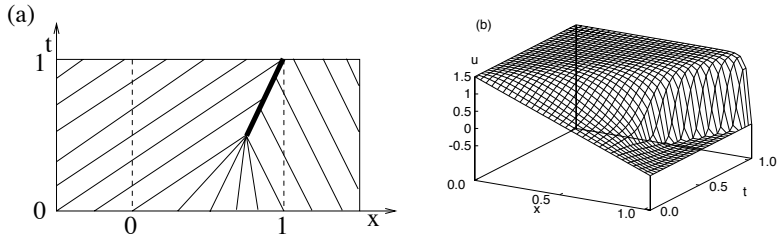

Figure 3.2: *Steepening of a linear profile into a shock for Burgers' equation. (a) Characteristic curves (thin solid) converge into the shock (thick solid). (b) Surface plot of u.*

The concept of characteristic curves carries over to a *system* of conservation laws with two independent variables in the following way.

Consider a *linear* system of n coupled equations

$$\frac{\partial \mathbf{U}}{\partial t} + \mathsf{A} \cdot \frac{\partial \mathbf{U}}{\partial x} = 0, \tag{3.27}$$

with $\mathbf{U}$ a state vector of n conserved quantities, and A a $n \times n$ constant matrix. Suppose an eigenvector decomposition of matrix $\mathsf{A} = \mathsf{R} \cdot \Lambda \cdot \mathsf{L}$ exists, with the columns of R being the right eigenvectors of A, the rows of L being the left eigenvectors of A, $\mathsf{R} = \mathsf{L}^{-1}$, and Λ being a diagonal matrix with the eigenvalues of A on the diagonal. The system is said to be hyperbolic if all the eigenvalues are real. The system can be described in terms of the *characteristic variables* $\mathbf{W} = \mathsf{L} \cdot \mathbf{U}$ as

$$\frac{\partial \mathbf{W}}{\partial t} + \Lambda \cdot \frac{\partial \mathbf{W}}{\partial x} = 0. \tag{3.28}$$

This decouples the equations, and for every component of $\mathbf{W}$ we have the conservation law

$$\frac{\partial w_i}{\partial t} + \lambda_i \frac{\partial w_i}{\partial x} = 0. \tag{3.29}$$

If the system is hyperbolic, then n families of characteristic curves exist in real space, defined by $dx/dt = \lambda_i$. These characteristics are straight lines, and each w_i is a RI on its associated family of characteristics. If some λ_i is complex, then its associated characteristic does not exist in real space, and it is said that the i^{th} characteristic field is elliptic.

A *nonlinear* system of n coupled equations in quasi-linear form with two independent variables is described by

$$\frac{\partial \mathbf{U}}{\partial t} + \mathsf{A}(\mathbf{U}) \cdot \frac{\partial \mathbf{U}}{\partial x} = 0, \tag{3.30}$$

— where $\mathsf{A}(\mathbf{U})$ can be the Jacobian matrix of a flux function $\mathbf{F}$ associated with a set of conservation laws — and is hyperbolic in state $\mathbf{U}$ if the eigenvector decomposition of $\mathsf{A}(\mathbf{U})$ exists and all the eigenvalues of $\mathsf{A}(\mathbf{U})$ are real. The definition of the characteristic variables $\partial\mathbf{W} = \mathsf{L}(\mathbf{U})\cdot\partial\mathbf{U}$ is now only locally valid. Characteristics exist if the system is hyperbolic, and the real eigenvalues of $\mathsf{A}(\mathbf{U})$ determine the slopes of the characteristics locally. The characteristics are in general not straight lines any more, except in *simple wave* regions, where one family of characteristics consists of straight lines [20, 85, 92]. Riemann Invariants do not generally exist, but sometimes it is possible to find one or more functions χ_i of the dependent variables $\mathbf{U}$ such that $d\chi_i \sim \mathsf{L}_i \cdot d\mathbf{U}$, which defines χ_i as a Riemann Invariant. The mathematical interpretation of characteristic curves is that derivatives normal to the characteristic curve cannot be determined from the governing equations, because the equations only specify derivatives along the characteristic curves. The solution on a characteristic curve does not determine the solution in neighboring points not on this curve. This geometric property puts strict constraints on the posing of boundary conditions, namely, that characteristic curves cannot serve as boundaries on which boundary conditions are imposed. The physical interpretation is that weak discontinuities propagate as waves along characteristics, such that a characteristic variable is locally conserved on its corresponding characteristic (whereas Riemann Invariants are globally conserved on their characteristics). Equivalently, the wave information carried by a local characteristic variable follows a strict characteristic path and cannot escape in a direction perpendicular to the characteristic. It does not influence the solution away from this characteristic.

The above analysis was placed in an xt context, and the theory of characteristics was related to concepts of propagation of physical waves in a time-dependent system. The same analysis can also be applied to steady state systems of equations, in which the time variable is not present anymore. Steady equations can also be hyperbolic, and by direct analogy we can relate the characteristic structure of steady equations to the stationary analogs of time-dependent waves, which we call stationary waves. For instance, the concept of simple waves in MHD can be carried over from the time-dependent context (xt) to the stationary context (xy) [85]. The formal analogy between the analysis of xt and xy systems of equations, both special cases of the full equations in xyt – or even $xyzt$ –, can be clarified by the following considerations. In the following Sections we use this formal analogy to derive the characteristic properties of the xt and xy MHD equations in a unified and systematic way.

A general quasi-linear time-dependent system of n first order partial

differential equations in two space dimensions is described by

$$\frac{\partial \mathbf{U}}{\partial t} + \mathsf{A}(\mathbf{U}) \cdot \frac{\partial \mathbf{U}}{\partial x} + \mathsf{B}(\mathbf{U}) \cdot \frac{\partial \mathbf{U}}{\partial y} = 0, \tag{3.31}$$

with $\mathbf{U}$ a vector of dependent variables and A and B $n \times n$ matrices. This system reduces to a system with two independent variables for the case of a 1D time-dependent flow ($\partial/\partial y = 0$) and for the case of a 2D steady flow ($\partial/\partial t = 0$). In the first case, the last term of Eq. 3.31 vanishes, and the procedure which was outlined above can be used to study the characteristic structure of the equations. In the second case, the first term of Eq. 3.31 vanishes, and one can examine the characteristic properties of the equation

$$\frac{\partial \mathbf{U}}{\partial x} + \mathsf{A}^{-1} \cdot \mathsf{B} \cdot \frac{\partial \mathbf{U}}{\partial y} = 0, \tag{3.32}$$

leading to characteristic analysis in the xy plane. The eigenvalues and left eigenvectors of the matrix $\mathsf{C} \equiv \mathsf{A}^{-1} \cdot \mathsf{B}$ again determine the type of the system, the characteristic directions in the xy plane, and the Riemann Invariants.

3.2.2 Characteristic analysis of time-dependent MHD in one space dimension

In this section, the above sketched general framework is applied to the MHD equations and a derivation is presented of some aspects of the characteristic theory of the MHD equations [21, 79, 59, 71, 85, 70, 3, 19]. We analyze the symmetrizable form of the equations (3.12), and do not use the condition $\nabla \cdot \vec{B} = 0$, unless where necessary and stated. In this way we are able to see how the characteristic structure of the MHD equations is independent of the $\nabla \cdot \vec{B}$ constraint, and when this constraint becomes important.

Equation 3.12 can be written in the quasi-linear form of Eq. 3.31 with $\mathbf{U} = (\rho, v_x, v_y, v_z, B_x, B_y, B_z, p)$ the vector of primitive variables, and matrices

$$\mathsf{A} = \begin{bmatrix} v_x & \rho & 0 & 0 & 0 & 0 & 0 & 0 \\ 0 & v_x & 0 & 0 & 0 & B_y/\rho & B_z/\rho & 1/\rho \\ 0 & 0 & v_x & 0 & 0 & -B_x/\rho & 0 & 0 \\ 0 & 0 & 0 & v_x & 0 & 0 & -B_x/\rho & 0 \\ 0 & 0 & 0 & 0 & v_x & 0 & 0 & 0 \\ 0 & B_y & -B_x & 0 & 0 & v_x & 0 & 0 \\ 0 & B_z & 0 & -B_x & 0 & 0 & v_x & 0 \\ 0 & c^2\rho & 0 & 0 & 0 & 0 & 0 & v_x \end{bmatrix}, \tag{3.33}$$

and

$$\mathsf{B} = \begin{bmatrix} v_y & 0 & \rho & 0 & 0 & 0 & 0 & 0 \\ 0 & v_y & 0 & 0 & -B_y/\rho & 0 & 0 & 0 \\ 0 & 0 & v_y & 0 & B_x/\rho & 0 & B_z/\rho & 1/\rho \\ 0 & 0 & 0 & v_y & 0 & 0 & -B_y/\rho & 0 \\ 0 & -B_y & B_x & 0 & v_y & 0 & 0 & 0 \\ 0 & 0 & 0 & 0 & 0 & v_y & 0 & 0 \\ 0 & 0 & B_z & -B_y & 0 & 0 & v_y & 0 \\ 0 & 0 & c^2\rho & 0 & 0 & 0 & 0 & v_y \end{bmatrix}. \quad (3.34)$$

The xt characteristic analysis yields the following results. The eigenvalues of matrix A are

$$\lambda_{1,2} = v_x \pm c_{fx}, \quad \lambda_{3,4} = v_x \pm c_{Ax}, \quad \lambda_{5,6} = v_x \pm c_{sx}, \quad \lambda_{7,8} = v_x. \quad (3.35)$$

Here c_{fx}, c_{Ax} and c_{sx} are the fast magneto-sonic wave speed, the Alfvén speed, and the slow magneto-sonic wave speed, which all depend on the direction x — they are *anisotropic*—, and which are given by

$$c_{fx}^2 = \frac{1}{2}\left(\frac{\gamma p + B^2}{\rho} + \sqrt{\left(\frac{\gamma p + B^2}{\rho}\right)^2 - 4\frac{\gamma p B_x^2}{\rho^2}}\right), \quad (3.36)$$

$$c_{Ax}^2 = \frac{B_x^2}{\rho}, \quad (3.37)$$

$$c_{sx}^2 = \frac{1}{2}\left(\frac{\gamma p + B^2}{\rho} - \sqrt{\left(\frac{\gamma p + B^2}{\rho}\right)^2 - 4\frac{\gamma p B_x^2}{\rho^2}}\right). \quad (3.38)$$

These wave speeds satisfy the property

$$c_{fx} \geq c_{Ax} \geq c_{sx}, \quad (3.39)$$

for any direction x. The hydrodynamic (HD) system has only one isotropic wave speed c, but the MHD system thus has three different wave modes which are highly anisotropic. In the direction of the magnetic field, the fast wave speed coincides with the largest of the sound and the Alfvén speed, while the slow wave speed coincides with the smallest of the two. Slow waves and Alfvén waves have a vanishing propagation speed in the direction perpendicular to the magnetic field. Slow and fast waves are called magneto-sonic waves, because they are compressible (ρ and p change) like sound waves in hydrodynamics. Compressibility is a nonlinear effect which can make fast and slow waves steepen into shocks. Alfvén waves are not compressible. They are linear waves.

We can define three Mach numbers associated with the three different wave modes. These Mach numbers also depend on the direction, and are

given by

$$M_{fx} = \frac{|v_x|}{c_{fx}}, \quad M_{Ax} = \frac{|v_x|}{c_{Ax}}, \quad \text{and} \quad M_{sx} = \frac{|v_x|}{c_{sx}}. \tag{3.40}$$

The eigenvalues in Eq. 3.35 are always real, meaning that the system is always hyperbolic, and the eigenvalues thus determine the characteristic directions in the xt plane. The left eigenvectors

$$\mathsf{L}_7 = (-c^2, 0, 0, 0, 0, 0, 0, 1) \text{ and } \mathsf{L}_8 = (0, 0, 0, 0, 1, 0, 0, 0), \tag{3.41}$$

can be used to derive the Riemann Invariants

$$\chi_7 = s \text{ and } \chi_8 = B_x. \tag{3.42}$$

For instance, the condition that $\mathsf{L}_7 \cdot d\mathbf{U} = 0$ in the direction of the characteristic with slope v_x, can be written as $\mathsf{L}_7 \cdot (d\rho, dv_x, dv_y, dv_z, dB_x, dB_y, dB_z, dp) = -c^2 d\rho + dp = 0$. This leads to $ds = 0$, because it follows from Eq. 3.9 that $ds = dp/\rho^\gamma - \gamma p/\rho^{\gamma+1}\, d\rho = (-c^2 d\rho + dp)/\rho^\gamma$. This means that the entropy s is a RI. Making use of $\nabla \cdot \vec{B} = 0$, it follows from Eq. 3.12 that B_x has to be constant in x and t, such that B_x is a global RI (with a constant value in the whole xt domain), and can thus be eliminated from the xt equations, resulting in the more common description of 1D time-dependent MHD with seven dependent variables. Here we can also clarify why we have started our analysis from Eq. 3.12 with the RHS term included: omission of this term results in an eigenvalue $\lambda_8 = 0$ [118], which is not a Galilean invariant property, because a change in reference frame would change v_x and thus all the wave speeds accordingly, except λ_8, which would remain zero also in the new reference frame. This zero eigenvalue makes matrix A singular, such that the general procedure outlined above to derive the xy characteristics, which uses A^{-1}, would fail.

3.2.3 Characteristic analysis of stationary MHD in two space dimensions

For steady state solutions the xy characteristic analysis yields the following results. In the stationary case, the governing equations are not always fully hyperbolic. If some eigenvalue of matrix $\mathsf{C} = \mathsf{A}^{-1} \cdot \mathsf{B}$ is not real, then its associated characteristic does not exist. It is hard to find closed expressions for the eigenvalues of matrix $\mathsf{C} = \mathsf{A}^{-1} \cdot \mathsf{B}$, but using software for symbolical calculation, we can easily factorize the condition $\det(\mathsf{C} - \lambda \mathsf{I}) = 0$ in terms of the variable

$$v_\perp^2 = \frac{(-v_y + v_x \lambda)^2}{1 + \lambda^2}, \tag{3.43}$$

which represents the square of the velocity component perpendicular to the characteristic, as the direction of the characteristic is given by $dy/dx = \lambda$. This factorization leads to the following roots:

$$v_{\perp 1}^2 = c_{f\perp}^2, \qquad v_{\perp 2}^2 = c_{A\perp}^2, \qquad v_{\perp 3}^2 = c_{s\perp}^2, \qquad v_{\perp 4}^2 = 0, \tag{3.44}$$

where $c_{f\perp}$, $c_{A\perp}$, and $c_{s\perp}$ are the fast magnetosonic, Alfvén, and slow magnetosonic velocities in the direction perpendicular to the characteristic [85, 19]. For every condition (3.44), if real λs can be found which satisfy the condition, then the associated characteristics exist and we say that the associated characteristic fields are hyperbolic.

The physical interpretation of these conditions is clear: if they exist, then the xy characteristics are curves from which no wave information carried by the associated characteristic variable can escape in a direction perpendicular to the characteristic. For instance, the wave with wave speed $v_\perp - c_{f\perp}$ perpendicular to the characteristic cannot transport information in this perpendicular direction when $v_\perp = c_{f\perp}$. This defines the steady xy characteristics as curves on which the perpendicular plasma speed equals a perpendicular wave speed. We say that the flow is sonic in the direction perpendicular to the characteristic.

The equation for $v_{\perp 4}$ always has two real solutions, $\lambda_{7,8} = v_y/v_x$, meaning that the streamlines are two-fold degenerate characteristics. The associated left eigenvectors are

$$\begin{aligned} \mathsf{L}_7 &= (-c^2, 0, 0, 0, 0, 0, 0, 1), \\ \mathsf{L}_8 &= (0, B_y/v_x, -B_x/v_x, 0, -v_y/v_x, 1, 0, 0), \end{aligned} \tag{3.45}$$

and can be used to derive the Riemann Invariants

$$\chi_7 = s \quad \text{and} \quad \chi_8 = -v_x B_y + v_y B_x = E_z, \tag{3.46}$$

with E_z the z-component of the electric field. Making use of $\nabla \cdot \vec{B} = 0$, it follows from (3.12) that Riemann Invariant $\chi_8 = E_z$ is a global invariant, as with $\nabla \cdot \vec{B} = 0$ the evolution equation of the magnetic field reduces to the classical form of the induction equation $\partial \vec{B}/\partial t = -\nabla \times \vec{E}$. Then $\partial \vec{B}/\partial t = -\nabla \times \vec{E} = 0$ leads to $\partial E_z/\partial x = \partial E_z/\partial y = 0$. E_z can thus be eliminated from the equations. The entropy is conserved on a streamline in continuous flow. However, it follows from the MHD Rankine-Hugoniot (RH) jump conditions [87, 92, 4], which are discussed in the next Section, that the entropy is discontinuous when a streamline crosses a shock.

The equation for $v_{\perp 2}$ always has two real solutions as well, $\lambda_{3,4} = (B_y \pm \sqrt{\rho} v_y)/(B_x \pm \sqrt{\rho} v_x)$.

The equations for $v_{\perp 1}$ and $v_{\perp 3}$ are much more complicated. Depending on the parameters, the equation for $v_{\perp 1}$ can have no solution or two solutions for λ. The equation for $v_{\perp 3}$ can have zero, two, or four real

solutions for λ, with the total number of real solutions for the two equations not exceeding four. The slow and fast magnetosonic characteristic fields can thus be hyperbolic or elliptic depending on the parameters, and no simple formulas can be found as criteria for hyperbolicity. Graphical methods can be used to determine the hyperbolic and elliptic regions of the equations [3, 79, 59, 71, 85, 70, 19].

In the case of planar MHD ($v_z \equiv B_z \equiv 0$), the Alfvén waves disappear, meaning that the families of characteristics corresponding to characteristic speeds λ_3 and λ_4 drop out, both in the xt and in the xy case. The other characteristic families remain unchanged.

For steady MHD in two space dimensions with no variation in the z direction, the xy plane is called the *poloidal plane*, and the velocity and magnetic fields in this plane are called the *poloidal* fields $\vec{v}^{(p)}$ and $\vec{B}^{(p)}$. If $\vec{v}^{(p)}$ and $\vec{B}^{(p)}$ are aligned somewhere in the xy domain, then $E_z = 0$ at that location. It then follows from the analysis given above, that $\vec{v}^{(p)}$ and $\vec{B}^{(p)}$ have to be aligned everywhere, as E_z is a global invariant and thus vanishes everywhere. It can be proved using the MHD RH relations, that this property is also conserved at shocks (as the tangential electric field is conserved at a shock). These properties establish the concept of steady *field-aligned* MHD flow, which is sometimes also called *parallel* flow. The above derived characteristic properties of stationary MHD in two space dimensions simplify considerably for the case of field-aligned flow, as is shown in the next Section. It is interesting to note that the characteristic structure of the MHD equations is independent of the constraint $\nabla \cdot \vec{B} = 0$. The characteristic structure derived from the symmetrizable form of the equations 3.12 is consistent and complete, without the need to impose the $\nabla \cdot \vec{B} = 0$ constraint. The concept of field-aligned flow, however, requires that $\nabla \cdot \vec{B} = 0$, because only then E_z is a global invariant.

3.2.4 Characteristic analysis of stationary field-aligned MHD in two space dimensions

The 2D MHD flows which we analyze in Chapters 5 and 6 of this dissertation belong to the class of steady planar field-aligned MHD. Therefore we now show how the above derived general results on characteristic analysis of the MHD equations simplify for the special cases of field-aligned flow and planar ($v_z \equiv B_z \equiv 0$) field-aligned flow [79, 59, 70, 62, 19].

We introduce the variable α in Eq. 3.12 with $\partial/\partial t = 0$ by taking $\vec{B}^{(p)} = \alpha \vec{v}^{(p)}$. The steady MHD equations for field-aligned flow reduce

then to a 7×7 system with $\mathbf{U} = (\rho, v_x, v_y, v_z, \alpha, B_z, p)$, and matrices

$$\mathsf{A} = \begin{bmatrix} v_x & \rho & 0 & 0 & 0 & 0 & 0 \\ 0 & v_x & \alpha^2 v_y/\rho & 0 & \alpha v_y^2/\rho & B_z/\rho & 1/\rho \\ 0 & 0 & (1-\alpha^2/\rho)v_x & 0 & -\alpha v_x v_y/\rho & 0 & 0 \\ 0 & 0 & 0 & v_x & 0 & -\alpha v_x/\rho & 0 \\ 0 & \alpha & 0 & 0 & v_x & 0 & 0 \\ 0 & B_z & 0 & -\alpha v_x & 0 & v_x & 0 \\ 0 & c^2\rho & 0 & 0 & 0 & 0 & v_x \end{bmatrix}, \tag{3.47}$$

and

$$\mathsf{B} = \begin{bmatrix} v_y & 0 & \rho & 0 & 0 & 0 & 0 \\ 0 & (1-\alpha^2/\rho)v_y & 0 & 0 & -\alpha v_x v_y/\rho & 0 & 0 \\ 0 & \alpha^2 v_x/\rho & v_y & 0 & \alpha v_x^2/\rho & B_z/\rho & 1/\rho \\ 0 & 0 & 0 & v_y & 0 & -\alpha v_y/\rho & 0 \\ 0 & 0 & \alpha & 0 & v_y & 0 & 0 \\ 0 & 0 & B_z & -\alpha v_y & 0 & v_y & 0 \\ 0 & 0 & c^2\rho & 0 & 0 & 0 & v_y \end{bmatrix}. \tag{3.48}$$

Note that, consistent with our earlier observations, the fifth row of the equations now automatically leads to $\nabla \cdot (\alpha \vec{v}) = \nabla \cdot \vec{B} = 0$, although we have only explicitly imposed that $\alpha \vec{v}^{(p)} = \vec{B}^{(p)}$, and not that $\nabla \cdot \vec{B} = 0$.

Analysis of the characteristic properties of this 7×7 system yields the following results. The characteristic condition $\det(\mathsf{C} - \lambda \mathsf{I}) = 0$ can be factorized in terms of λ. This factorization leads to the following roots

$$\lambda_{1,2} = \frac{1}{B^2 + \rho\,(c^2 - v_x^2) - c^2 B^{(p)2}/v^{(p)2}} (-\rho v_x v_y \pm \sqrt{\left(B^2 + \left(\rho - B^{(p)2}/v^{(p)2}\right) c^2\right) \left(\rho v^{(p)2} - B^2 - \left(\rho - B^{(p)2}/v^{(p)\,2}\right) c^2\right)}), \tag{3.49}$$

$$\lambda_{3-7} = \frac{v_y}{v_x}. \tag{3.50}$$

Here B^2 is the squared magnitude of the total magnetic field, and $B^{(p)2}$ and $v^{(p)2}$ are the squared magnitudes of the poloidal fields.

The $\lambda_{3-7} = v_y/v_x$ are always real and thus correspond to hyperbolic fields with associated characteristics, which means that the poloidal streamlines are five-fold degenerate characteristics. A basis for the corresponding left eigenvector space is

$$\mathsf{L}_3 = (-c^2, 0, 0, 0, 0, 0, 1) \tag{3.51}$$

$$\mathsf{L}_4 = (-\alpha/\rho, 0, 0, 0, 1, 0, 0) \tag{3.52}$$

$$\mathsf{L}_5 = (B_z/(\alpha^2 - \rho), 0, 0, 0, 0, 1, 0) \tag{3.53}$$

$$\mathsf{L}_6 = (\alpha B_z/(\alpha^2\rho - \rho^2), 0, 0, 1, 0, 0, 0) \tag{3.54}$$

$$\mathsf{L}_7 = (\frac{B_z^2 + c^2(-\alpha^2+\rho)}{\rho v_y(-\alpha^2+\rho)}, \frac{v_x}{v_y}, 1, 0, 0, 0, 0), \tag{3.55}$$

and can be used to derive the Riemann Invariants

$$\chi_3 = s = \frac{p}{\rho^\gamma} \tag{3.56}$$

$$\chi_4 = \rho/\alpha \tag{3.57}$$

$$\chi_5 = L = \frac{B^{(p)}B_z}{\rho v^{(p)}} - v_z \tag{3.58}$$

$$\chi_6 = \Omega = \frac{v^{(p)}B_z}{B^{(p)}} - v_z = \frac{E}{B^{(p)}} \tag{3.59}$$

$$\chi_7 = h = \frac{v^2}{2} + \frac{\gamma}{\gamma-1}\frac{p}{\rho} - v_z B_z \frac{B^{(p)}}{\rho v^{(p)}} + \frac{B_z^2}{\rho}, \tag{3.60}$$

with s the entropy, L related to the angular momentum, Ω related to the electric field, h the Bernoulli function and E the magnitude of the electric field.

The invariance of these quantities along streamlines can also be derived by direct manipulation of the conservation laws of Eq. 3.12. For instance, using $\nabla \cdot \vec{B} = 0$ and $\vec{B}^{(p)} = \alpha\vec{v}^{(p)}$, one can see that $\nabla \cdot (\rho\vec{v}) = \nabla \cdot (\rho/\alpha\ \alpha\vec{v}) = \alpha\vec{v} \cdot \nabla(\rho/\alpha) + \rho/\alpha\ \nabla \cdot (\alpha\vec{v}) = \alpha\vec{v} \cdot \nabla(\rho/\alpha)$. Because $\nabla \cdot (\rho\vec{v}) = 0$ in a steady state, this leads to $\vec{v} \cdot \nabla(\rho/\alpha) = 0$, which means that ρ/α is conserved on a streamline.

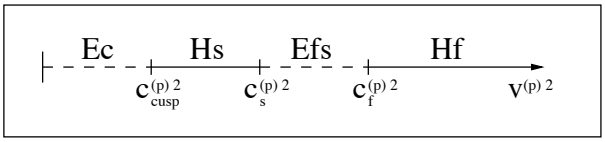

Figure 3.3: *Elliptic and hyperbolic regions in parameter space for steady field-aligned MHD. For decreasing $v^{(p)2}$, the axis is divided in a fast hyperbolic region (Hf), an elliptic region between the fast and the slow hyperbolic regions (Efs), a slow hyperbolic region (Hs), and an elliptic region below the cusp speed (Ec).*

The eigenvalues $\lambda_{1,2}$ are real and the equations are thus hyperbolic if the factor under the square root sign is positive [79, 59, 71, 85, 70, 3, 62, 19]. This factor changes sign three times, viz. when the square of the poloidal velocity equals

$$v^{(p)2} = c_{f,s}^{(p)2} = \frac{B^2 + \gamma p \pm \sqrt{(B^2+\gamma p)^2 - 4B^{(p)2}\gamma p}}{2\rho} \tag{3.61}$$

$$v^{(p)2} = c_{cusp}^{(p)2} = \frac{c_A^{(p)2} c^2}{c_A^2 + c^2}. \tag{3.62}$$

Here $c_A = B/\sqrt{\rho}$ is the total Alfvén velocity, and $c_A^{(p)} = B^{(p)}/\sqrt{\rho}$ is the poloidal Alfvén velocity. The poloidal cusp velocity $c_{cusp}^{(p)}$ is the velocity of the slow wave cusp in the MHD Friedrichs diagram [59, 71]. This leads to a division of the parameter space into elliptic and hyperbolic regions, as depicted in Fig. 3.3. Note that the poloidal Alfvénic Mach number $M_A^{(p)}$ becomes independent of the direction for the case of field-aligned flow:

$$M_{Ax} = \frac{|v_x|}{c_{Ax}} = M_{Ay} = \frac{|v_y|}{c_{Ay}} = M_A^{(p)} = \frac{v^{(p)}}{c_A^{(p)}}. \tag{3.63}$$

3.2.5 Characteristic analysis of stationary planar field-aligned MHD in two space dimensions

In the *planar* case ($v_z \equiv B_z \equiv 0$) the results simplify further. We can simplify the notation by dropping the superscripts (p), e. g. $c_A^{(p)} = c_A$ and $v^{(p)} = v$. The matrices A and B given in Eqs. 3.47 and 3.48 lose their fourth and sixth rows and columns. Analysis of the characteristic properties of the resulting 5×5 system yields the following results. The characteristic condition $\det(\mathsf{C} - \lambda \mathsf{I}) = 0$ can be factorized in terms of the variable $v_\perp^2$. This factorization leads to the following roots

$$v_{\perp 1}^2 = c^2(1 - \alpha^2/\rho) + v^2\ \alpha^2/\rho \qquad \text{and} \qquad v_{\perp 2}^3 = 0. \tag{3.64}$$

The equation for $v_{\perp 2}$ always has three real solutions, $\lambda_{3,4,5} = v_y/v_x$, meaning that the streamlines are three-fold degenerate characteristics. The corresponding left eigenvectors are

$$\begin{aligned} \mathsf{L}_3 = (-c^2, 0, 0, 0, 1)\ \ , \ \ \mathsf{L}_4 = (-\alpha/\rho, 0, 0, 1, 0)\ \ , \\ \text{and}\ \ \mathsf{L}_5 = (c^2/(\rho v_y), v_x/v_y, 1, 0, 0), \end{aligned} \tag{3.65}$$

and can be used to derive the Riemann Invariants

$$\chi_3 = s\ \ , \ \ \chi_4 = \rho/\alpha\ \ , \text{ and } \ \chi_5 = h_s. \tag{3.66}$$

The hydrodynamic stagnation enthalpy is defined as

$$h_s \equiv \frac{\gamma}{\gamma - 1}\frac{p}{\rho} + \frac{1}{2}v^2. \tag{3.67}$$

The entropy, ρ/α, and the stagnation enthalpy are thus conserved on a streamline in continuous flow. It follows from the MHD Rankine-Hugoniot (RH) jump conditions [87, 92, 4], that the entropy is discontinuous when a streamline crosses a shock. However, the stagnation

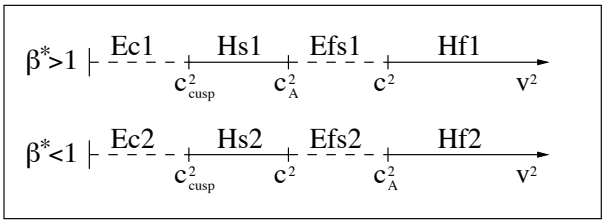

Figure 3.4: *Elliptic and hyperbolic regions in parameter space for steady planar field-aligned MHD. The top line corresponds to* $\beta^* > 1$*, and shows, as* v^2 *decreases, a division in a fast hyperbolic region (Hf1), an elliptic region between the fast and the slow hyperbolic regions (Efs1), a slow hyperbolic region (Hs1), and an elliptic region below the cusp speed (Ec1). The bottom line shows a similar division for* $\beta^* < 1$*. For* $\beta^* = 1$*,* $c^2 = c_A^2$*.*

enthalpy and ρ/α are conserved over a shock for the case of field-aligned flow.

The solutions of the equation for $v_{\perp 1}$ are

$$\lambda_{1,2} = \frac{\rho v_x v_y \pm \sqrt{(v^2 - c^2)(\alpha^2 - \rho)(c^2(\alpha^2 - \rho) - v^2\alpha^2)}}{\rho(c^2 - v_x^2) - \alpha^2(c^2 - v^2)}. \qquad (3.68)$$

If the factor under the square root sign is positive, then these eigenvalues are real, and the equations are hyperbolic [79, 59, 71, 85, 70, 3, 62, 19]. This factor changes sign three times, viz. when the square of the velocity equals

$$v^2 = c_A^2, \qquad v^2 = c^2, \qquad \text{and} \qquad v^2 = c_{cusp}^2. \qquad (3.69)$$

The cusp velocity is defined as $c_{cusp}^2 = (c^2 c_A^2)/(c^2 + c_A^2)$ and is the velocity of the slow wave cusp in the MHD Friedrichs diagram [59, 71]. This leads to a division of the parameter space into elliptic and hyperbolic regions, as depicted in Fig. 3.4, for high and low β^*, where the parameter β^* is defined as $\beta^* = \gamma p/B^2 = c^2/c_A^2$. When $\beta^* > 1$ — or equivalently $\beta > 2/\gamma = 1.2$ — the sound speed is larger than the Alfvén speed, or, equivalently, thermal pressure effects dominate over magnetic pressure effects.

In Fig. 3.5a the local geometry of streamlines and xy characteristics is sketched for the case of planar steady field-aligned MHD in hyperbolic regions. The streamline is a three-fold degenerate characteristic, and there are two additional families of characteristics (generalized Mach lines [21, 20]) which make equal angles ψ with the streamline. These characteristics can be of the slow or fast type, depending on which hyperbolic regime the parameters are in (Hf or Hs of Fig. 3.4). Division of

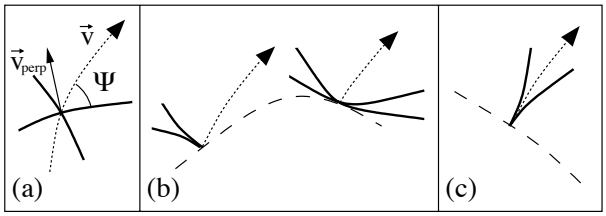

Figure 3.5: *Streamlines (dotted), slow or fast characteristics (thick), and transition lines between hyperbolic and elliptic regions (dashed), for steady planar field-aligned MHD. (a) The two families of characteristics (thick) both make an angle ψ with the streamline. (b) At transition lines where the plasma velocity equals the sound speed or the Alfvén speed, the characteristics become perpendicular to the streamline. When the streamline is perpendicular to the transition line, the characteristics are tangent to the transition line. (c) At transition lines where the plasma velocity equals the cusp speed, the characteristics cusp and are tangent to the streamline.*

the expression for $v_{\perp 1}^2$ in Eq. 3.64 by v^2 leads to the following interesting formula for the angle ψ between the streamline and the characteristic (Fig. 3.5a):

$$\sin^2\psi = \frac{v_\perp^2}{v^2} = \frac{M^2 + M_A^2 - 1}{M^2 M_A^2}. \tag{3.70}$$

The total sonic Mach number $M = v/c$ has to be distinguished from the directional Mach number $M_x = |v_x|/c$. The Alfvénic Mach number M_A is independent from the direction. The flow is hyperbolic when $0 \leq (M^2 + M_A^2 - 1)/(M^2 M_A^2) \leq 1$. For $v^2 = c_A^2$ ($M_A^2 = 1$) or $v^2 = c^2$ ($M^2 = 1$), $v_\perp^2$ equals v^2 and $\psi = 90°$, meaning that at such transition lines between elliptic and hyperbolic regions, the characteristics are perpendicular to the streamlines, as is shown in Fig. 3.5b. At transition lines of these types, characteristics can thus only be parallel to these lines when the streamline is perpendicular to the transition line. For $v^2 = c_{cusp}^2$, $v_\perp^2$ equals zero and $\psi = 0°$, meaning that at this type of transition line between elliptic and hyperbolic regions, the characteristics cusp parallel to the streamlines [62, 131], as is shown in Fig. 3.5c.

In some cases further simplifications can be made. If the stagnation enthalpy is the same on every streamline (this is called homenthalpic flow), then p can be eliminated from the equations, resulting in a 4×4 system with state vector $\mathbf{U} = (\rho, v_x, v_y, \alpha)$. In this case λ_5 and χ_5 drop out, but the rest of the analysis remains the same. Similarly, steady planar hydrodynamics in 2D results in a 4×4 system with $\mathbf{U} = (\rho, v_x, v_y, p)$. The results for this special case of vanishing magnetic field are recovered

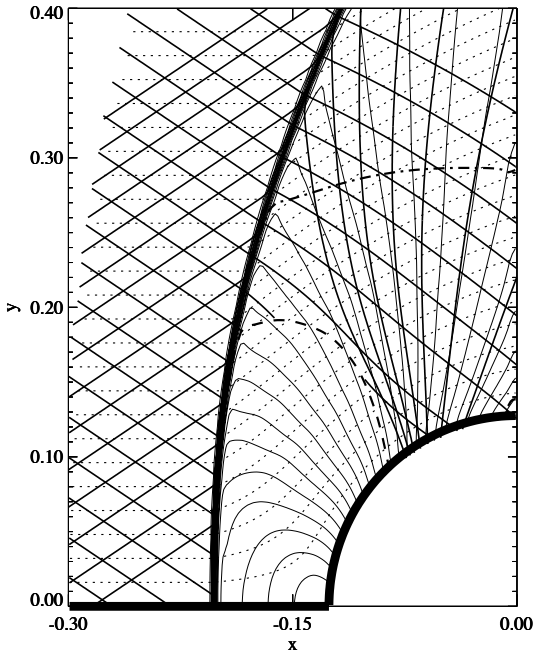

Figure 3.6: *Planar field-aligned 2D MHD bow shock flow over a perfectly conducting plate with a semi–circular bump (thick). The flow comes in from the left. Density contours (thin solid lines) pile up in the shock. The streamlines (which are also magnetic field lines) are dotted. The thick solid lines are two families of fast characteristics making equal angles with the streamlines. The thick dashed transition line is the $M = 1$ contour, separating the elliptic region close to the cylinder (Efs1) from the rest of the flow, which is fully hyperbolic (Hf2 and Hf1). The fast characteristics are perpendicular to the streamlines at the transition line. The thick dash-dotted line is the $\beta^* = 1$ contour.*

by putting $\alpha = 0$ in the formulas for planar field-aligned MHD, in which case λ_4 and χ_4 drop out.

To illustrate the above derived results, we show the characteristics of a planar 2D MHD bow shock flow in Fig. 3.6. The flow comes in from the left ($\rho = 1$, $p = 0.2$, $v_x = 2$, $v_y = 0$, $B_x = 1$, $B_y = 0$), and is obstructed by the perfectly conducting cylinder on the right. Due to top-down symmetry, this setting can also be thought of as to describe the flow over a perfectly conducting plate with a semi–circular bump (thick). Density contours (thin solid lines) pile up in the shock. The streamlines (which

Table 3.1: Overview of some characteristic properties of the MHD equations, for full (8×8) MHD in the xt and the xy planes, and for steady field-aligned MHD (7×7 and planar 5×5) in the xy plane. The first column labels the characteristic fields as in the text. The second column gives the characteristic directions λ or the condition on $v_\perp$ for every characteristic field. The third column gives the Riemann Invariants. The fourth column gives the multiplicity of the real eigenvalues, and thus indicates if the corresponding characteristic fields are hyperbolic or elliptic.

characteristic field	λ **or** $v_\perp$	**RI**	**multiplicity**
xt (8×8)			
1,2	$\lambda = v_x \pm c_f$		2
3,4	$\lambda = v_x \pm c_A$		2
5,6	$\lambda = v_x \pm c_s$		2
7,8	$\lambda = v_x$	$s,\ B_x$	2
xy (8×8)			
1,2	$v_\perp^2 = c_{f\perp}^2$		0—2
3,4	$v_\perp^2 = c_{A\perp}^2$		2
5,6,1,2	$v_\perp^2 = c_{s\perp}^2$		0—2—4
7,8	$v_\perp^2 = 0$	$s,\ v_xB_y - v_yB_x$	2
xy, $\vec{B}^{(p)} \parallel \vec{v}^{(p)}$ (7×7)			
1,2	$\lambda_{1,2}$		0—2
3,4,5,6,7	$v_\perp^5 = 0$	$s,\ \rho/\alpha,\ L,\ \Omega,\ h$	5
xy, $\vec{B} \parallel \vec{v}$ (5×5)			
1,2	$\lambda_{1,2}$		0—2
3,4,5	$v_\perp^3 = 0$	$s,\ \rho/\alpha,\ h_s$	3

are also magnetic field lines) are dotted. The thick solid lines are two families of fast characteristics making equal angles with the streamlines in the hyperbolic regions. In front of the cylinder we see an elliptic region, where the thick characteristics do not exist. We can determine the types of the hyperbolic and elliptic regions in the flow according to the classification given in Fig. 3.4. The parameter β^* is smaller than one upstream, and greater than one downstream from the shock, except far away from the cylinder (the thick dash-dotted line is the $\beta^* = 1$ contour). The thick dashed transition line is the $M = 1$ contour, separating the subsonic elliptic region close to the cylinder (Efs1) from the rest of the flow, which is supersonic and thus hyperbolic (Hf2 upstream from the shock and downstream far from the cylinder, and Hf1 downstream and

closer to the cylinder). The fast characteristics are perpendicular to the streamlines at the transition line, corresponding to case (b) of Fig. 3.5.

A summary of the results on characteristic analysis of the MHD equations with two independent variables is given in Table 3.1. This characteristic theory is applied to the analysis of numerically obtained model flow solutions in Chapter 5, and to complex 2D bow shock flow solutions in Chapter 6.

As a final remark, we can note that the concepts of characteristic analysis can be extended to systems with three and four independent variables [21, 169]. The matter becomes quite more complicated, and necessitates the introduction of concepts like characteristic rays, surfaces, and cones. For the analysis of numerical results presented further on in this dissertation, however, it is not necessary to consider systems with more than two independent variables.

3.3 MHD discontinuities

3.3.1 MHD Rankine-Hugoniot relations

Consider the ideal MHD equations in one space dimension. These equations allow for solutions composed of a uniform left state and a uniform right state which are connected by a discontinuity, and this discontinuity moves with a constant speed s and has a magnitude which is constant in time. In the frame moving with speed s, the solution is thus stationary, and we call such a solution a co-stationary discontinuous traveling wave. We can easily derive the general conditions which must be fulfilled by such a co-stationary discontinuous traveling wave solution, and verify if those conditions can indeed be satisfied in the case of the MHD system. In general, a conservation law system

$$\frac{\partial \mathbf{U}(x,t)}{\partial t} + \frac{\partial \mathbf{F}(\mathbf{U})}{\partial x} = 0 \tag{3.71}$$

allows for a co-stationary traveling wave solution $\mathbf{U}(x,t) = \mathbf{U}(y = x - st)$ under the condition that

$$-s\frac{\partial \mathbf{U}(y)}{\partial y} + \frac{\partial \mathbf{F}(\mathbf{U})}{\partial y} = 0, \tag{3.72}$$

or

$$-s\mathbf{U} + \mathbf{F}(\mathbf{U}) = \mathbf{F}_{const} \tag{3.73}$$

with $\mathbf{F}_{const}$ a constant vector [173, 46]. In particular, for the *discontinuous* co-stationary traveling wave solution described above, the left and right states $\mathbf{U}_l$ and $\mathbf{U}_r$ thus have to satisfy the condition

$$\mathbf{F}(\mathbf{U}_r) - \mathbf{F}(\mathbf{U}_l) = s\ (\mathbf{U}_r - \mathbf{U}_l), \tag{3.74}$$

which expresses that the physical fluxes have to be continuous through the discontinuity in the moving frame. This can be seen more clearly when we transform to that moving frame and rewrite Eq. 3.74 as

$$\mathbf{F}(\mathbf{U}_r) = \mathbf{F}(\mathbf{U}_l). \tag{3.75}$$

Conditions 3.74 or 3.75 are called the *Rankine-Hugoniot* (RH) relations. We have to remark here that for a discontinuous solution, the derivatives in the differential form of the conservation law Eq. 3.71 are not defined. The discontinuous solution is, however, a valid solution of the integral form of the conservation law Eq. 3.73, and we say that it is a *weak solution* of the differential form of the conservation law Eq. 3.71. The RH relations actually have to be satisfied by any traveling discontinuity in the ideal system (not only by co-stationary solutions), because they describe the conservation of the physical fluxes through the discontinuity interface. The RH relations can alternatively be derived from Eq. 3.71 by applying Gauss' law on a volume which is cut by a plane shock and by taking the limit of vanishing thickness of the volume, such that the time derivative integrated over the volume vanishes as well. This can be done because the shock has vanishing thickness in the ideal system.

The MHD flux function in the x direction is given by

$$F\left(\begin{bmatrix} \rho \\ \rho v_x \\ \rho v_y \\ \rho v_z \\ B_x \\ B_y \\ B_z \\ e \end{bmatrix}\right) = \begin{bmatrix} \rho v_x \\ \rho v_x^2 + p + B^2/2 - B_x^2 \\ \rho v_x v_y - B_x B_y \\ \rho v_x v_z - B_x B_z \\ 0 \\ B_y v_x - B_x v_y \\ B_z v_x - B_x v_z \\ (e + p + B^2/2) v_x - B_x \, (\vec{v} \cdot \vec{B}) \end{bmatrix}. \tag{3.76}$$

This flux function allows for several different types of co-stationary discontinuous traveling wave solutions each with their particular properties. The derivation of these properties from the MHD RH relations would lead us too far here, and is well described elsewhere [4, 87, 80]. We just give a short overview of some results that are used later. We assume the x direction to be perpendicular to the shock, and the magnetic field to lie in the xy plane.

MHD discontinuities can be divided in three classes. For shocks there is both a mass flow through the surface of discontinuity, and an increase in the entropy. For contact and tangential discontinuities, there is an entropy jump, but no mass flow. For rotational discontinuities, there is a mass flow, but no entropy change. A general property of MHD discontinuities is that the normal component of the magnetic field B_x is continuous, as follows directly from the $\nabla \cdot \vec{B} = 0$ constraint.

3.3.2 Shocks

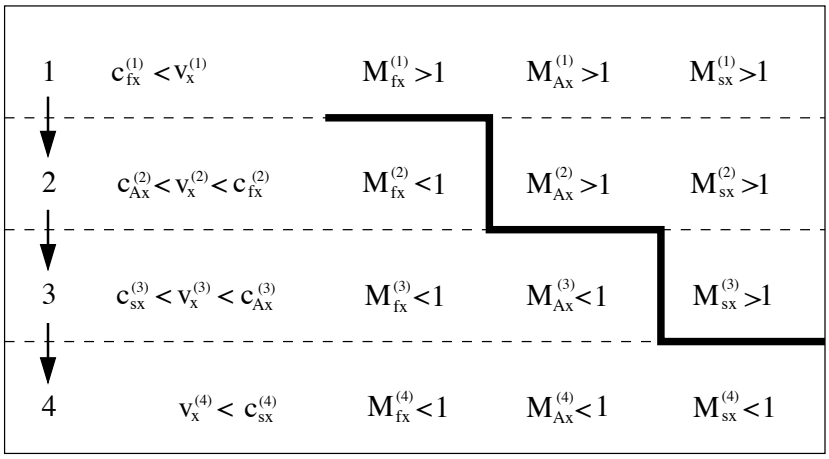

Figure 3.7: *Possible states that can be connected through a MHD shock. They are ordered by increasing entropy, with the lowest entropy for state 1. The normal fast, Alfvén, and slow wave speeds are c_{fx}, c_{Ax}, and c_{sx}, respectively. The normal plasma speed is v_x. The fast, Alfvén, and slow normal Mach numbers are M_{fx}, M_{Ax}, and M_{sx}, respectively. State 1 is superfast, because its normal velocity in the shock frame is larger than the normal fast MHD wave speed. Therefore the fast, Alfvénic and slow Mach numbers are all greater than one. State 2 is subfast but super-Alfvénic. State 3 is sub-Alfvénic but superslow. State 4 is subslow. Possible shock transitions are 1–2 (fast), 3–4 (slow), and 1–3, 1–4, 2–3, 2–4 (intermediate).*

A general property of MHD shocks is that the left and the right state are *co-planar*. This means that the plane defined by the shock normal and the magnetic field is the same plane on both sides of the shock. This property can easily be derived from the MHD RH relations. Another property is that if the magnetic field and velocity field are parallel on one side of a shock, then the fields are also parallel on the other side of the shock.

Generally up to four plasma states can be found that satisfy given values for the fluxes of mass, momentum, magnetic field and energy through the discontinuity surface. This follows from analysis of the RH conditions [87, 80]. Each pair of those states satisfies the RH conditions and can thus be connected by a shock. These states are conventionally labeled states 1, 2, 3, and 4, ordered by increasing entropy (Fig. 3.7). State 1 has the lowest entropy, and in a frame moving with the shock

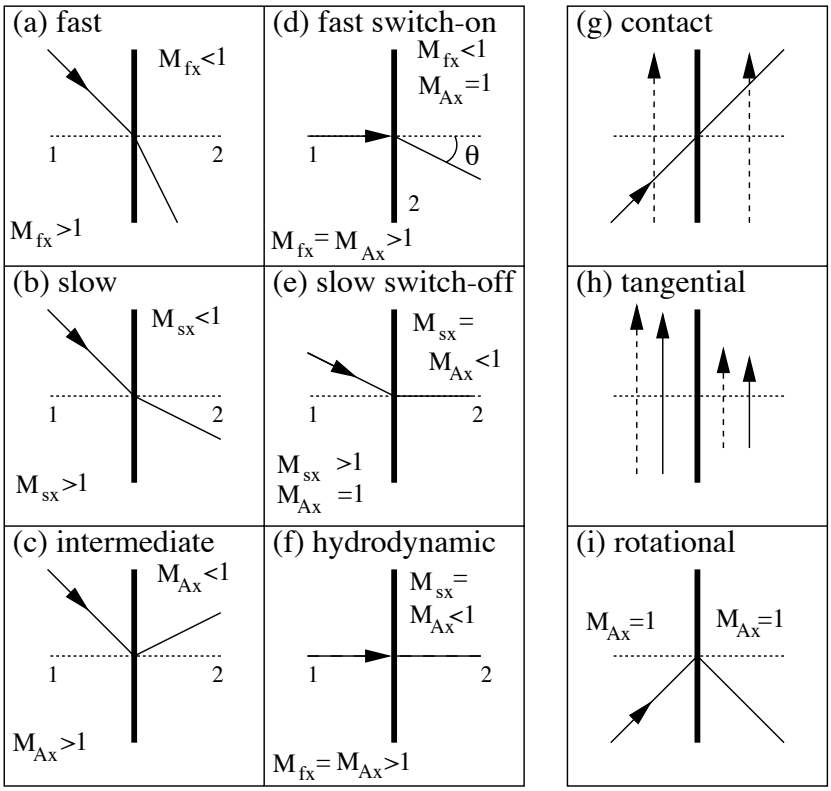

Figure 3.8: *Some properties of MHD shocks and discontinuities. The thick vertical line is the shock surface. The shock normal is dotted. The full arrowed lines are magnetic field lines that are refracted through the shock surface. The dashed arrowed lines are velocity vectors. Region 1 is upstream, 2 is downstream.*

the normal plasma velocity $v_x^{(1)}$ is larger than the normal fast MHD wave speed, so that the flow is superfast (and, therefore, also super-Alfvénic and superslow). This means that the normal fast Mach number $M_{fx}^{(1)}$ (normal plasma velocity divided by normal fast MHD wave speed) is greater than one (the same for the Alfvén and slow Mach number). State 2 is subfast, but super-Alfvénic and superslow. State 3 is subfast and sub-Alfvénic, but superslow. State 4 is subfast, sub-Alfvénic, and subslow. In a frame of reference that moves with the shock, a fluid element that moves from the upstream region (traditionally indicated as region 1) to the downstream region (region 2), necessarily has to undergo an increase in entropy. So 1–2, 1–3, 1–4, 2–3, 2–4, and 3–4 are the

possible entropy-satisfying shock transitions. In Fig. 3.8 we summarize some of their properties.

Transition 1–2 is called a fast shock (Fig. 3.8a). The plasma is superfast upstream, and subfast (but super-Alfvénic) downstream. A fast shock increases B_y (because p is in phase with B for a fast wave), such that magnetic field lines are refracted away from the shock normal. Transition 3–4 is called a slow shock (Fig. 3.8b). The plasma is superslow (but sub-Alfvénic) upstream, and subslow downstream. A slow shock decreases B_y (because p is in anti-phase with B for a slow wave), such that magnetic field lines are refracted towards the shock normal. Transitions 1–3, 1–4, 2–3, and 2–4 are called intermediate shocks (Fig. 3.8c). The plasma is super-Alfvénic upstream, and sub-Alfvénic downstream. An intermediate shock changes the sign of B_y, such that magnetic field lines are flipped over the shock normal.

There exist limiting cases of these types of shocks for which the upstream and/or downstream magnetic field is parallel to the shock normal. A fast 1–2=3 switch-on shock (Fig. 3.8d) has $B_{y,1} = 0$ upstream. The downstream $B_{y,2}$, however, does not vanish. The tangential component of the magnetic field is thus switched on, hence the name of this shock. For a fast switch-on shock, the downstream normal Alfvénic Mach number is exactly equal to one. A slow 2=3–4 switch-off shock (Fig. 3.8e) has $B_{y,2} = 0$ downstream. The upstream $B_{y,1}$ however does not vanish. The tangential component of the magnetic field is thus switched off, hence the name of this shock. For a slow switch-off shock, the upstream normal Alfvénic Mach number is exactly equal to one. A limiting case of intermediate shocks are shocks that do not change the magnetic field, and those shocks are called 1–4 hydrodynamic (or parallel) shocks (Fig. 3.8f). Both $B_{y,1}$ and $B_{y,2}$ are equal to zero.

Intermediate shocks and switch-on shocks can only occur for some well-specified regime of the upstream parameters [80, 147]. For switch-on shocks, the downstream angle θ (Fig. 3.8d) is non-vanishing only if the upstream plasma $\beta_1 < 2/\gamma$ and if the upstream normal velocity component $v_{x,1}$ lies in the switch-on region between the upstream Alfvén speed and a critical velocity defined by

$$c_{A,1} < v_{x,1} < c_{A,1}\sqrt{\frac{\gamma(1-\beta_1)+1}{\gamma-1}} = v_{crit}. \tag{3.77}$$

The upstream tangential component of the velocity, $v_{y,1}$, does not play a role in condition 3.77. In fact, one can always make a transformation to a new frame in the direction tangential to the shock front, and choose the new frame such that $v_{y,1} = 0$. The magnetic field does not change in this transformation of frames. The shock properties can then be analyzed in this new frame. The parameter regime for which switch-on

shocks occur is called the *switch-on regime*. Intermediate shocks arise for the same parameter regime, and can only exist when the angle between the upstream magnetic field and the shock normal is small, as will be illustrated shortly.

Switch-on shocks have no analog in the hydrodynamic flow of a neutral fluid, and can thus be called an intrinsically magnetic effect. A plasma state upstream from a shock with the magnetic field normal to the shock is a superfast state — type 1 — if $v_{x,1} > c_1$ and $v_{x,1} > c_{A,1}$, or equivalently

$$\rho_1 v_{x,1}^2 > \gamma p_1 \tag{3.78}$$

and

$$\rho_1 v_{x,1}^2 > B_1^2. \tag{3.79}$$

Here $v_{x,1}$ is the velocity component along the shock normal and along the upstream magnetic field. The 1–2 shock with this state of type 1 as upstream state is a switch-on shock when

$$B_1^2 > \gamma p_1 \tag{3.80}$$

and

$$B_1^2 > \rho_1 v_{x,1}^2 \frac{\gamma - 1}{\gamma(1-\beta_1)+1}. \tag{3.81}$$

The latter inequality can be deduced from Eq. 3.77. The expression $(\gamma - 1)/(\gamma(1 - \beta_1) + 1)$ assumes values between 0.25 and 1 for $\gamma = 5/3$ and $\beta_1 < 2/\gamma$. Eqs. 3.80 and 3.81 show that switch-on shocks occur when magnetic forces dominate over the effects from both the thermal pressure p and the dynamic pressure $\rho v_x^2/2$ in the direction normal to the shock. Switch-on shocks can only occur when the magnetic field B is strong and are an intrinsically magnetic effect. Therefore we call upstream flows for which switch-on shocks can occur *magnetically dominated* flows. Magnetically dominated flows thus satisfy inequalities 3.78-3.81. Upstream flows for which switch-on shocks do not occur are called *pressure-dominated* flows.

Fast switch-on shocks and the parameter regime in which they occur, which we call the magnetically dominated regime, play an important role in Chapters 6, 7 and 8 of this dissertation. It is shown that for upstream parameters in this magnetically dominated regime bow shock flows exhibit a new complex topology which is very different from the traditional topology obtained for bow shocks with pressure-dominated upstream flows. This motivates the introduction of the terminology of pressure-dominated versus magnetically dominated upstream flows as defined above, and warrants its extension to pressure-dominated versus magnetically dominated bow shock flows and bow shock flow topologies. Full justification for this terminology is given in Secs. 6.3 and 7.1.

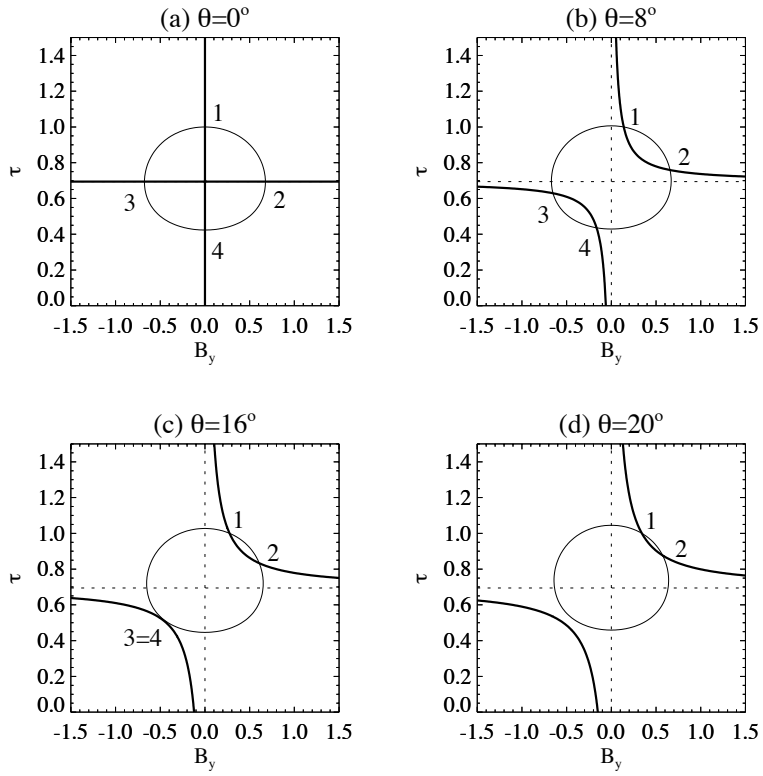

Figure 3.9: *Solutions of the RH relations for parameter values $M_A = 1.2$ and $\beta = 0.4$ for state 1 with the field aligned to the flow. These are magnetically dominated parameters for which switch-on shocks occur. θ is the angle between the fields and the shock normal. (a) For $\theta = 0°$, switch-on shocks, switch-off shocks and hydrodynamic shocks arise. (b–d) For $\theta < 16°$, intermediate shocks occur, but they cease to exist for larger θ.*

We can illustrate the above discussion on MHD shocks by explicitly plotting solutions of the RH conditions for given values of the fluxes through the discontinuity. We follow closely the procedure described in [4]. For given fluxes through the discontinuity, up to four states satisfying the RH relations can be found as the intersection of two curves in the $\tau - B_y$ plane, with $\tau = 1/\rho$ and B_y the component of the magnetic field tangential to the shock surface. The shock normal is again taken in the x direction.

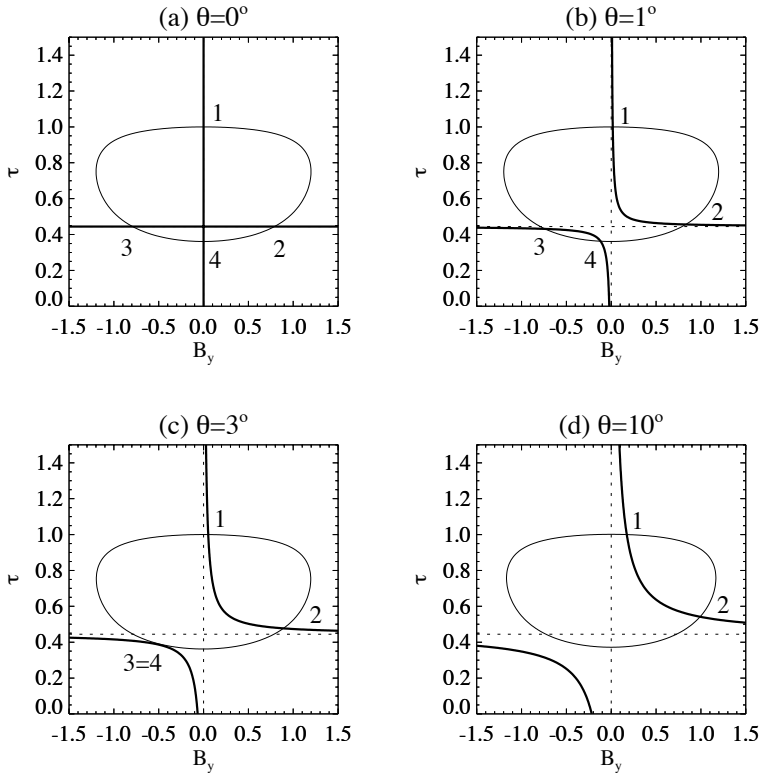

Figure 3.10: *Solutions of the RH relations for parameter values $M_A = 1.5$ and $\beta = 0.4$ for state 1 with the field aligned to the flow. These parameters still are magnetically dominated, but not strongly. The maximum angle for which intermediate shocks can occur is smaller than for the parameter values of Fig. 3.9.*

Fig. 3.9 shows RH solutions for parameter values $p = 0.2$, $\rho = 1$, $B = 1$ and $v = 1.2$ for state 1. The velocity is taken parallel to the magnetic field. We vary the angle θ between the aligned velocity and magnetic field vectors, and the shock normal. In state 1 $c_A = 1$, $M_A = 1.2$ and $\beta = 0.4$. β is smaller than $2/\gamma = 1.2$ and, for $\theta = 0°$, $v_x < v_{crit} = 1.732$ (Eq. 3.77). Intermediate and switch-on shocks occur, and we call the upstream state magnetically dominated.

Fig. 3.9b, for $\theta = 8°$, shows the generic case with four solutions of the RH relations. The horizontal dotted line indicates the inverse density

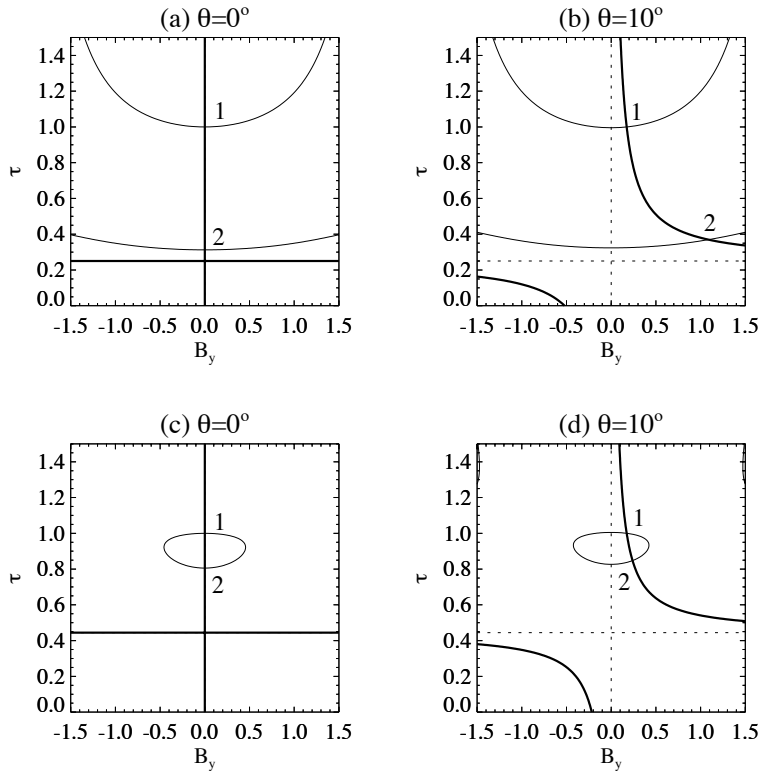

Figure 3.11: *Solutions of the RH relations for pressure-dominated parameter values for state 1. Switch-on shocks do not occur. Only 1–2 fast shocks exist. (a–b)* $M_A = 2$ *and* $\beta = 0.4$*. (c–d)* $M_A = 1.5$ *and* $\beta = 2$*.*

τ for which $v_x = c_{Ax}$. 1–2 is a fast shock (B_y increases), and 3–4 is a slow shock (B_y decreases). Transitions 1–3, 1–4, 2–3 and 2–4 all cross the $v_x = c_{Ax}$ line, and are thus intermediate shocks, which is confirmed by the fact that they change the sign of the B_y component.

Fig. 3.9a shows the limiting case for $\theta = 0°$. 1–2 and 1–3 are both fast switch-on shocks (B_y is switched on), and because states 2 and 3 are both Alfvénic ($v_x = c_{Ax}$), this type of shock is referred to as a 1–2=3 shock. The 2=3–4 shocks are slow switch-off shocks. The 1–4 shock is a hydrodynamic shock ($\vec{B}$ does not change through the shock). Figs. 3.9c and d show that for angles θ larger than approximately 16° intermediate shocks cease to exist.

Fig. 3.10 shows RH solutions for the same parameter values for state

1 as in Fig. 3.9, except that $v = 1.5$ and thus closer to $v_{crit} = 1.732$. The upstream state is still magnetically dominated as switch-on shocks can still occur — remark that the switch-on angle ($\approx B_y$) even has increased! —, but the maximum angle for which intermediate shocks occur decreases to $\theta \approx 3°$. This is a generic property: when v_x is taken closer to v_{crit}, the maximum angle for which intermediate shocks can occur decreases. This behavior can also be observed in Fig. 3 of [80] and Fig. 4 of [147].

Fig. 3.11 shows RH solutions for parameter values for state 1 not in the switch-on regime — we call the upstream state thus pressure-dominated. Fig. 3.11a–b shows RH solutions for the same parameter values for state 1 as in Fig. 3.9, except that $v = 2$ and thus exceeds $v_{crit} = 1.732$. This means that dynamic pressure effects dominate over magnetic effects — inequality 3.81 is not satisfied. Only 1–2 fast shocks exist. In Fig. 3.11c–d, $p = 1$, $\rho = 1$, $B = 1$ and $v = 1.5$. $\beta = 2$, such that thermal pressure effects dominate over magnetic effects — inequality 3.80 is not satisfied. Again only fast shocks exist.

3.3.3 Other discontinuities

Contact discontinuities (Fig. 3.8g), with vanishing v_x but nonzero B_x, have only a jump in density (and entropy). All other quantities are continuous. Tangential discontinuities (Fig. 3.8h), with vanishing v_x and B_x, have a jump in density, pressure, and tangential velocity and magnetic field. However, the total pressure $p + B^2/2$ is continuous. Planar rotational discontinuities (Fig. 3.8i) rotate the magnetic field around the normal of the discontinuity surface over an angle of 180 degrees, without a jump in entropy. Rotational discontinuities can actually rotate the magnetic field over an arbitrary angle, and the planar rotational discontinuity is just a special case. The normal plasma velocity v_x equals $B_x/\rho^{1/2}$ on both sides of a rotational discontinuity, such that the normal Alfvénic Mach number equals one on both sides. Transitions 2–3 in Figs. 3.9a and 3.10a are planar rotational discontinuities which are the limit of intermediate 2–3 shocks for zero shock strength.

3.3.4 Stability of shocks

All the types of discontinuities discussed above formally satisfy the MHD RH relations, but there exists a vigorous debate about the physical relevance of some of these types of discontinuities, notably the intermediate shocks and the rotational discontinuities. This is discussed in detail in Chap. 9. In the mean time, we refer the reader to the discussion in Sec. 2.3.2, where it was indicated that intermediate shocks can be stable in small dissipation MHD. We will thus not be surprised when intermediate

shocks appear in our simulation results presented in Chapters 6, 7 and 8, but thorough discussion of the relevance of these results for the debate on the existence of intermediate shocks is postponed to Chap. 9.

3.3.5 Non-convexity and MHD compound shocks

In this Section we show how the non-convexity of characteristic fields leads to the occurrence of compound shocks. Large parts of our exposition derive from material presented in [90] and [173].

Let us first consider the *scalar* conservation law Eq. 3.23. A *Riemann problem* is an initial value problem with an initial condition in the form of a step discontinuity with uniform states to the left and the right of the discontinuity. Fig. 3.12a and b shows the solution of a Riemann problem for the scalar conservation law with flux function $f(u) = u^2/2$, which is called the inviscid Burgers equation, and with left and right states $u_l = 1$ and $u_r = -1$. We can investigate if these two states can be connected by a co-stationary discontinuous traveling wave solution (a traveling shock). From Eq. 3.74 we can derive that the shock speed would equal $s = (f(u_r) - f(u_l))/(u_r - u_l) = 0$.

For now we adopt the — naive, see Chap. 9 — criterion that shocks are admissible when the characteristics enter the shock on both sides. We assume that if the characteristics do not enter the discontinuity on both sides — such discontinuities are called *undercompressive* —, then the discontinuity is not stable and cannot be formed. Physically this criterion corresponds to the fact that the entropy has to increase at a shock, as is explained in Chap. 9 [90].

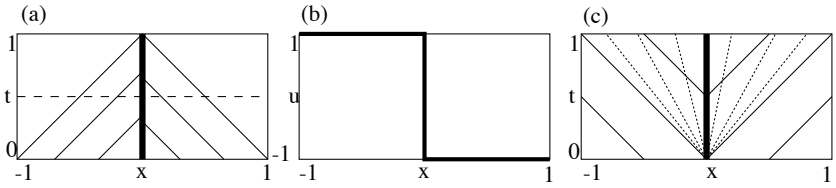

Figure 3.12: *Solution of a Riemann problem for the inviscid Burgers equation. (a) Left and right states $u_l = 1$ and $u_r = -1$ lead to an admissible shock (thick solid) with speed $s = 0$ and characteristics (thin solid) converging into the shock. (b) Shock profile of the solution presented in (a) for $t = 1/2$. (c) Left and right states $u_l = -1$ and $u_r = 1$ do not allow for a shock, because the characteristics leave the shock. Instead, a centered rarefaction (dotted) results.*

In Fig. 3.12 we see that a shock with left and right states $u_l = 1$ and $u_r = -1$ is an admissible shock, because the characteristics converge

into the shock. The solution of the Riemann problem is thus given by a shock solution which happens to be stationary in the frame considered. If we switch the left and the right states, we find the same shock speed $s = 0$, but a shock clearly would be undercompressive and thus inadmissible, as shown in Fig. 3.12c. In stead of a shock, we find a *centered rarefaction wave* which broadens in time as the solution of the Riemann problem (indicated by the dotted lines in the figure). The admissibility of rarefactions is, of course, not questionable, because they are regular continuous solutions.

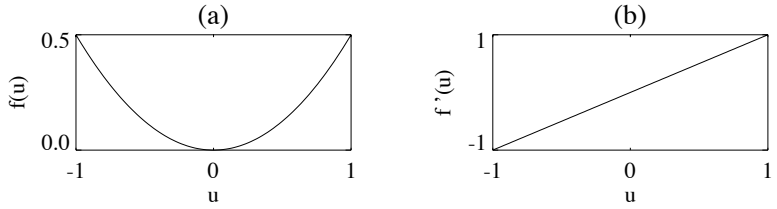

Figure 3.13: *Flux function $f(u)$ and characteristic speed function $f'(u)$ for Burgers' equation. $f(u)$ is convex because $f'(u)$ is monotone.*

Figs. 3.13a and b show plots of the flux function $f(u)$ and the characteristic speed function $f'(u)$ for Burgers' flux function $f(u) = u^2/2$. This flux function is called *convex* because $f'(u)$ is monotone, or, equivalently, $f''(u)$ does not change sign. This property is important, because it guarantees that every Riemann problem can be solved either with an admissible traveling shock or with a rarefaction. Indeed, given two states u_1 and u_2, with the indices chosen such that $f'(u_1) > f'(u_2)$, the property of convexity guarantees that $f'(u_1) \geq s = (f(u_2) - f(u_1))/(u_2 - u_1) \geq f'(u_2)$, which means that states $u_l = u_1$ and $u_r = u_2$ can be connected by an admissible shock. If the left and the right states are switched, the solution to the Riemann problem would consist of a rarefaction between two constant states. If f were non-convex, then the shock speed s would *not* be guaranteed to lie between the characteristic speeds of the two states, so pairs of states would exist which could never be connected by an admissible shock.

So what happens with the Riemann problem in the case of a *non-convex* flux function? Fig. 3.14 shows the solution of a Riemann problem for the non-convex scalar conservation law with flux function $f(u) = u^3/3$, and with left and right states $u_l = 1$ and $u_r = -3/4$. Fig. 3.15a and b show plots of the flux function $f(u)$ and the characteristic speed function $f'(u)$ for the flux function $f(u) = u^3/3$. Clearly $f'(u)$ is not monotone, and the flux function is thus non-convex. For these left and

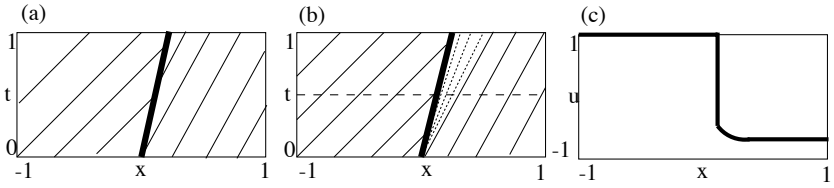

Figure 3.14: *Solution of a Riemann problem for the scalar conservation law with flux function* $f(u) = u^3/3$. *(a) Left and right states* $u_l = 1$ *and* $u_r = -3/4$ *do not allow for an admissible shock, because the characteristics leave the shock on the right. (b) The solution of the Riemann problem consists of a compound shock, composed of a sonic shock followed by an attached centered rarefaction. (c) Shock profile of the solution presented in (b) for* $t = 1/2$.

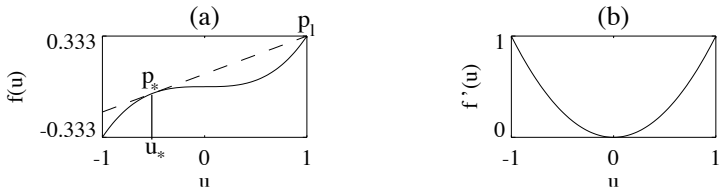

Figure 3.15: *Flux function* $f(u) = u^3/3$ *and characteristic speed function* $f'(u)$. $f(u)$ *is non-convex because* $f'(u)$ *is not monotone. In a compound shock, the right state* u_* *of the shock is chosen such that it can be connected to* $u_l = 1$ *by a sonic shock, with the characteristic parallel to the shock. To this end the straight line connecting* p_l *and* p_* *has to be tangent to the curve* $f(u)$ *in point* p_*.

right states, the shock speed $s = 37/168 = 0.22$, and the characteristic speeds are $f'(u_l) = 1$ and $f'(u_r) = 9/16$, such that $f'(u_l) \geq f'(u_r) \geq s$. The shock is thus undercompressive, as shown in Fig. 3.14a. A rarefaction solution is not possible either, because the characteristics intersect. So we have to look for a different type of solution for this case of a non-convex flux function.

It turns out that the solution of Fig. 3.14b and c is admissible. It consists of a shock with a rarefaction attached, and with the peculiar property that the characteristic is parallel to the shock where the rarefaction is attached to the shock. This combined shock-rarefaction structure is called a *compound shock*. The compound shock solution can be constructed as follows. In Fig. 3.15a we fix the point p_l on the curve

corresponding to the left state $u_l = 1$. We can connect this point to any other point on the curve with a straight line, and the slope of this line gives the speed of the shock which could connect the states corresponding to the two points on the curve. This is precisely the geometrical interpretation of relation Eq. 3.74. We now connect p_l to the point p_* on the curve (at $u = -1/2$) such that the straight line connecting the two points is *tangent* to the curve. We choose $u_* = -1/2$, and connect u_l with u_* via a shock, with shock speed $s = 1/4$. This shock speed s is also equal to the characteristic speed $f'(u_*)$ in state u_*, because the straight line connecting u_l and u_* is tangent to the curve in u_*, and because the characteristic speed is given by the slope of the curve $f(u)$, and the shock speed by the slope of the straight line. The shock connecting u_l and u_* is thus admissible, because the characteristic enters the shock on the left, and is parallel to the shock on the right.

We call the shock *sonic* because the shock speed equals the characteristic speed on one side of the shock. State u_* can then be connected to state u_r by a continuous rarefaction. What happens if we switch u_l and u_r? In this case a solution with a single shock or rarefaction is not possible either, because the characteristics cross and would enter the shock on one side, but leave the shock on the other side. So again we find that a compound shock is necessary. This compound shock can be constructed by drawing a line now starting from the point corresponding to $u = -3/4$ (because the characteristics originating from this state enter the shock) and tangent to the curve $f(u)$.

We can thus conclude that non-convexity leads to the occurrence of compound shocks in solutions of Riemann problems. Compound shocks are composed of a sonic shock with an attached rarefaction which broadens in time, as shown in Fig. 3.14c for $t = 1/2$. The characteristic is parallel to the shock on the sonic side.

We can also have another look at the property of non-convexity which allows us to make the link with the MHD case. We follow the reasoning presented in [173]. Eq. 3.73 describes the propagation of co-stationary traveling waves, and the scalar version reads

$$-su + f(u) = f_{const} \tag{3.82}$$

We ask ourselves how many solutions Eq. 3.82 has for u, for given shock speed s and flux constant f_{const}, and whether admissible shocks with shock speed s exist which connect the solutions. For the convex Burgers flux function $f(u) = u^2/2$ this equation has zero or two real solutions, and the shock speed s always lies between the characteristic speeds of the two solutions, such that an admissible shock can always be constructed connecting the two solutions. For the non-convex flux function $f(u) = u^3/3$, however, Eq. 3.82 has 1 or 3 real solutions. The sum of these roots vanishes, such that if there are three roots, two roots have the same sign,

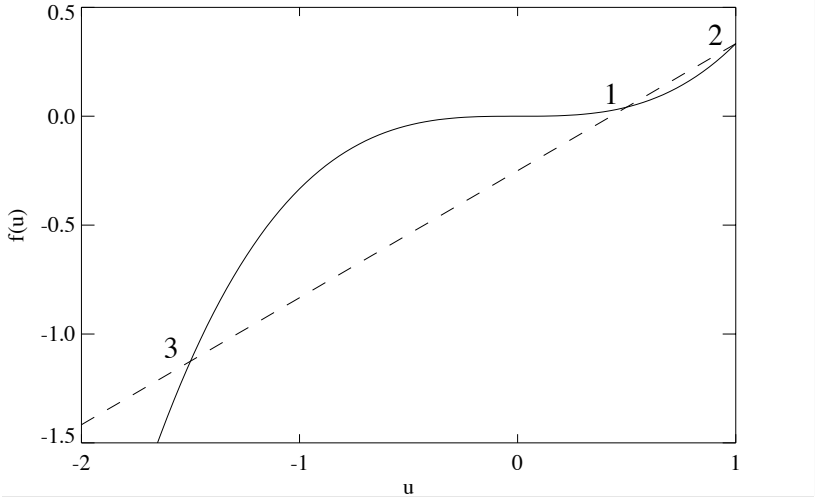

Figure 3.16: *Three solutions exist for the scalar conservation law with non-convex flux function* $f(u) = u^3/3$ *and for* $s = 7/12$ *and* $f_{const} = -3/12$ *. State 1 and 2 have the same sign, and state 3 has the opposite sign.*

and the third one has the opposite sign. Let us label those first two roots 1 and 2, with root 1 of the smaller magnitude, and let us give the label 3 to the root with the opposite sign. For instance, and as shown in Fig. 3.16, for $s = 7/12$ and $f_{const} = -3/12$, we find $u = 1/2$ for state 1, $u = 1$ for state 2 and $u = -1.5$ for state 3. We now investigate if the pairs of solutions (1,2), (1,3) and (2,3) can be connected by admissible shocks with speed s.

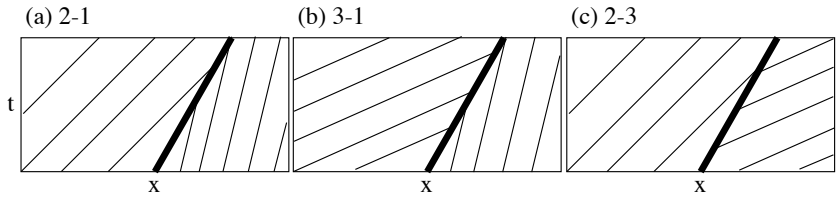

Figure 3.17: *Possible shock connections between the fixed points of Fig. 3.16. (a-b) Connections 2–1 and 3–1 are admissible shocks. (c) Pair (2,3) cannot be connected by an admissible shock.*

Fig. 3.17 shows that pair (1,2) can indeed be connected by an admissible shock 2–1, with state 2 on the left and state 1 on the right. Pair (1,3) can also be connected by a 3–1 shock. Pair (2,3), however, cannot be connected by an admissible shock. The shock with shock speed s is undercompressive in this case. We see thus that the non-convex case is very different from the convex case. In the convex case, there is just one type of admissible shock. In the non-convex case, we see that there are *two different types of admissible shocks* associated with just *one characteristic field*. The 1–2 (or 2–1) shock does *not* change the sign of the scalar u, and we could call it a *regular* shock. The 1–3 (or 3–1) shock *does* change the sign of the scalar u, and we could call it an *intermediate* shock. According to this definition, shock 2–3 (or 3–2) is also of the intermediate type, but this shock is undercompressive and thus inadmissible.

For the compound shock of Figs. 3.14 and 3.15, states 1 and 2 coincide, so the compound shock is composed of a 3–1=2 sonic intermediate shock followed by an attached rarefaction. The fact that 1=2 in the right state (u_*) precisely makes the shock sonic.

We can thus learn from this analysis that non-convexity allows for several different types of shocks associated with a single characteristic field. Alternatively, we could also say that different types of shocks are encountered when Eq. 3.82 has more than two real solutions [173].

The concept of a compound shock carries over to the separate non-convex characteristic fields of *systems* of hyperbolic equations. At least one family of characteristics has to converge into a shock on both sides in order to have an admissible shock. In the case of a 1D Riemann problem, the attached rarefaction is a simple wave, with the consequence that one family of characteristics in the rarefaction consists of straight lines [20, 85, 92]. This family of characteristics is parallel to the shock on the sonic side. Brio and Wu [12] show that the MHD flux function is not convex for the fast and the slow characteristic fields, and they encounter compound shocks in numerical solutions of 1D MHD Riemann problems. Myong and Roe [109, 110] show that compound shocks are essential elements for the solution of some planar ($v_z \equiv B_z \equiv 0$) MHD Riemann problems.

The properties of the MHD shock system 1–2–3–4 can be related to the shock properties of the scalar non-convex equation described above. This has been done rigorously by several authors who derive 'model systems' by simplifying the MHD equations [81, 109, 110, 46]. Here we have to restrict ourselves to suggesting some of the analogies and stating some important results. The non-convex fast characteristic field of MHD can be thought of as to allow for shock states labeled 1–2–3, and the non-convex slow field gives rise to states 2–3–4. These three states are in both instances analogous to the three states associated with the

scalar non-convex flux function $f(u) = u^3/3$. The change of sign of u can be associated with the change of sign of the tangential component of the magnetic field B_y, and the MHD intermediate shocks 1–3 and 2–4 are analogous to the scalar intermediate shock 1–3. In MHD, however, the fast and the slow characteristic fields are 'merged together' in a 1–2–3–4 system, and this merged system contains other degenerate phenomena in addition to the compound shock phenomenon. A fast MHD compound shock contains a 1=2–3 shock, with $v_x = c_{fx}$ upstream, analogous to the 1=2–3 sonic intermediate shock in the scalar compound shock described above. Analogously, a slow MHD compound shock contains a 2–3=4 shock, with $v_x = c_{sx}$ on the downstream side of the shock.

This analysis thus shows that compound shocks can arise in MHD flows. They were indeed encountered in numerical simulations of 1D MHD Riemann problems, but they have never been found in 2D or 3D simulations of realistic flow problems. In Chapters 6 and 7 we investigate bow shock flows with magnetically dominated upstream parameters for the presence of compound shocks.

Another interesting conclusion follows from the above analysis. It seems that the intermediate shocks are associated to the non-convex fast and slow modes, and *not* to the Alfvén mode, as could be expected intuitively. This explains for instance why intermediate shocks can arise in planar MHD flows while there are no Alfvén waves in planar MHD. This also explains the following contradiction. We have suggested that nonlinearity is necessary for the steepening of shocks, for instance in our description of the steepening of profiles for the Burgers equation in Fig. 3.2. However, the Alfvén characteristic field is a *linearly degenerate* field [90], or, equivalently, the Alfvén waves are not compressible. (It is exactly the compressibility which makes the fast and slow waves nonlinear and steepening.) But then how can intermediate shocks steepen if they are associated with a linearly degenerate field?

Part of the answer is that 1–3 and 2–4 intermediate shocks are not associated with the Alfvén characteristic field, but rather with the fast and the slow fields. We have to mention here that linearly degenerate fields can also 'carry' discontinuous waves, but those discontinuities are not 'self-steepening' and thus more prone to (turbulent) instability. They are not shocks (in the MHD context), because there is no entropy change or no mass flow across them. For instance, the entropy field is linearly degenerate, and the associated discontinuities are contact discontinuities, which do not steepen, but can form for instance downstream of λ-points where three shock branches meet in 2D flows. Chap. 6 shows some examples of this. The linearly degenerate Alfvén field has *rotational discontinuities* as associated discontinuous waves. These rotational discontinuities do not steepen. This picture is interesting but too simple, because 2–3 intermediate shocks can also directly be associated

with the Alfvén mode [41].

We can thus conclude that 1–3 and 2–4 intermediate shocks are not the discontinuous solutions directly associated with the Alfvén mode. However, there is certainly a relationship between these intermediate shocks and Alfvén waves and Alfvén speeds, because intermediate shocks satisfy the proper Alfvén Mach number inequalities (Figs. 3.8 and 3.7). This complex behavior is related to the fact that the MHD system is non-strictly hyperbolic (wave speeds can coincide). We come back to issues like this in Chap. 9.